

# CE-DYNAM (v1), a spatially explicit, process-based carbon erosion scheme for the use in Earth system models

Victoria Naipal<sup>1,2</sup>, Ronny Lauerwald<sup>3</sup>, Philippe Ciais<sup>2</sup>, Bertrand Guenet<sup>2</sup>, Yilong Wang<sup>2</sup>

<sup>1</sup>Ludwig-Maximilians University, Munich, Germany

<sup>2</sup>Laboratoire des Sciences des Sciences du Climat et de l'Environnement, CEA CNRS UVSQ, Gif-sur-Yvette 91191, France

<sup>3</sup>Department of Geoscience, Environment and Society, Université Libre de Bruxelles, Brussels, Belgium

*Correspondence* : Victoria Naipal (vnaipal24@gmail.com)

**Abstract.** Soil erosion by rainfall and runoff is an important process behind the redistribution of soil organic carbon (SOC) over land, hereby impacting the exchange of carbon (C) between land, atmosphere and rivers. However, the net role of soil erosion in the global C cycle is still unclear as it involves small-scale SOC removal, transport and re-deposition processes that can only be addressed over selected small regions with measurements and models. This leads to uncertainties in future projections of SOC stocks and complicates the evaluation of strategies to mitigate climate change through increased SOC sequestration.

In this study we present the parsimonious process-based Carbon Erosion DYNAMics model (CE-DYNAM) that links sediment dynamics resulting from water erosion with the C cycle along a cascade of hillslopes, floodplains and rivers. The model simulates horizontal soil and C transfers triggered by erosion across landscapes and the resulting changes in land-atmosphere CO<sub>2</sub> fluxes at a resolution of about 8 km at the catchment scale. CE-DYNAM is the result of the coupling of a previously developed coarse-resolution sediment budget model and the ecosystem C cycle and erosion removal model derived from the ORCHIDEE land surface model. CE-DYNAM is driven by spatially explicit historical land use change, climate forcing, and global atmospheric CO<sub>2</sub> concentrations affecting ecosystem productivity, erosion rates and residence times of sediment and C in deposition sites. The main features of CE-DYNAM are (1) the spatially explicit simulation of sediment and C fluxes linking hillslopes and floodplains, (2) the relative low number of parameters that allow running the model at large spatial scales and over long-time scales, and (3) its compatibility with global land surface models, hereby, providing opportunities to study the effect of soil erosion under global changes.

We present the model structure, concepts, limitations and evaluation at the scale of the Rhine catchment for the period 1850-2005 AD. Model results are validated against independent estimates of gross and net soil and C erosion rates, and the spatial variability of SOC stocks from high-resolution modeling studies and observational datasets. We show that despite local differences, the resulting soil and C erosion rates, and SOC stocks from CE-DYNAM are comparable to high-resolution estimates and observations at sub-basin level.

35  
36 We find that soil erosion mobilized around  $66\pm 28$  Tg ( $10^{12}$  g) of C under changing climate and land use over the  
37 non-Alpine region of the Rhine catchment, assuming that the erosion loop of the C cycle was in near steady-state by 1850.  
38 This caused a net C sink equal to 2.1-2.7% of the Net Primary Productivity of the non-Alpine region over 1850-2005 AD.  
39 This sink is a result of the dynamic replacement of C on eroding sites that increases in this period due to rising atmospheric  
40 CO<sub>2</sub> concentrations enhancing the litter C input to the soil from primary production.

41  
42 **Keywords.** soil erosion; regional carbon cycle; carbon sink; Rhine catchment; regional modelling

## 43 44 **1 Introduction**

45  
46 Soils contain more carbon (C) than the atmosphere and living biomass together. Relatively small disturbances  
47 (anthropogenic or natural) to soil C pools over large areas could add up to substantial C emissions (Ciais et al., 2013). With  
48 the removal of natural vegetation and the introduction of mechanized agriculture, humans have accelerated soil erosion  
49 rates. Over the last two to three decades, studies have shown that water erosion (soil erosion by rainfall and runoff)  
50 amplified by human activities has substantially impacted the terrestrial C budget (Doetterl et al., 2012; Lal, 2003; Lugato et  
51 al., 2018; Van Oost et al., 2007, 2012; Stallard, 1998; Wang et al., 2017). However, the net effect of water erosion on the C  
52 cycle at regional to global scale is still under debate. This leads to uncertainties in the future projections of the soil organic  
53 C (SOC) reservoir, and complicates the evaluation of strategies to mitigate climate change by increased SOC sequestration.  
54 The study of Stallard (1998) was one of the first to show that water erosion does not only lead to additional C emissions  
55 but can also sequester C due to the photosynthetic replacement of SOC at eroding sites and the stabilization of SOC in  
56 deeper layers at burial sites. The study of van Oost et al. (2007) was the first to confirm the importance of the sequestration  
57 of SOC by agricultural erosion at global scale using isotope tracers. Wang et al. (2017) gathered data on SOC profiles from  
58 erosion and deposition sites and confirmed that water erosion on agricultural land that started from the early/middle  
59 Holocene has caused a large net global land C sink. Other studies, however, argue that soil erosion is a net C source to the  
60 atmosphere due to increased SOC decomposition following soil aggregate breakdown during transport and at deposition  
61 sites (Lal et al, 2003; Lugato et al., 2018). Most studies modeling soil erosion and its net effect on SOC dynamics at global  
62 scale, however, did not account for the full range of complex effects of climate change, CO<sub>2</sub> fertilization increasing  
63 productivity and potentially soil C inputs, harvest of biomass, land use change, and changes in cropland management. In  
64 addition, models used at large spatial scales mainly focus on hillslopes and removal processes and neglect floodplain  
65 sediment and SOC dynamics. This can lead to substantial biases in the assessment of net effects of SOC erosion at  
66 catchment scale because floodplains can store substantial amounts of sediment and C (Berhe et al., 2007; Hoffmann et al.,  
67 2013a). Studies addressing long-term large-scale sediment yield from hillslopes and floodplains, such as Pelletier et al.  
68 (2012), do not explicitly account for the redistribution of sediment and SOC over land.

69

70 Furthermore, soil erosion is one of the main contributors to particulate organic carbon (POC) fluxes in rivers and C export  
71 to the coastal ocean. The riverine POC fluxes are usually much smaller than the SOC erosion fluxes, because only a small  
72 fraction of eroded material is entering the river network, while POC losses occur in the river network and due to  
73 decomposition and burial in floodplains and in benthic sediments (Tan et al., 2017; Galy et al., 2015). Therefore,  
74 uncertainties in large-scale SOC erosion rates will lead to even larger uncertainties in lateral C fluxes between land and  
75 ocean for past and future scenarios estimated by global empirical models on riverine C export (Ludwig and Probst, 1998;  
76 Mayorga et al., 2010).

77  
78 To address these knowledge gaps, we present a parsimonious process-based Carbon Erosion Dynamics Model  
79 (CE-DYNAM), which integrates sediment dynamics resulting from water erosion with the SOC dynamics at the regional  
80 scale. The SOC dynamics are calculated consistently with drivers of land use change, CO<sub>2</sub> and climate change by a  
81 process-based land surface model (LSM), with a simplified reconstruction of the last century increase of crop productivity.  
82 This modelling approach consists of a global sediment budget model coupled to the SOC removal, input, and  
83 decomposition processes diagnosed from the ORCHIDEE global LSM in an offline setting (Naipal et al., 2018). The main  
84 aim of our study is to quantify the horizontal transport of sediment and C along the continuum of hillslopes, floodplains  
85 and rivers, and at the same time analyze its impacts on the land-atmosphere C exchange. We validate the new model with  
86 regional observations and high-resolution modelling results of the Rhine catchment. It should be noted here that the  
87 structure of CE-DYNAM is designed in a way that the model can be adapted easily to other large catchments and finally  
88 run globally. We also discuss the model uncertainties and the sensitivity of the model to changes in key model parameters  
89 and assumptions made. In the next sections we give a detailed overview of the CE-DYNAM model structure, the coupling  
90 of erosion, deposition and transport with the coarse-resolution SOC dynamics of ORCHIDEE, model application and  
91 validation for the non-Alpine region of the Rhine catchment, and its potentials and limitations.

## 92 93 **2 Methods**

### 94 95 **2.1 General model description**

96  
97 CE-DYNAM version 1 (v1) is the result of coupling a large-scale erosion and sediment budget model (Naipal et al., 2016)  
98 with the SOC scheme of the land surface model ORCHIDEE (Krinner et al., 2005). The most important features of the  
99 model are (1) the spatially explicit simulation of lateral sediment and C transport fluxes over land linking hillslopes and  
100 floodplains, (2) consistent simulation of vertical C fluxes coupled with horizontal transport, (3) the low number of  
101 parameters compared to other C erosion models that operate at a high spatial resolution (Lugato et al., 2018; Billings et al.,  
102 2019) that allows running the model at large spatial scales and over time-scales up to several thousands of years, (4) the  
103 generic input fields for application to any region or catchment, and (5) compatibility with land surface models (LSMs).

105 In the ORCHIDEE LSM, terrestrial C is represented by eight biomass pools, four litter pools and three SOC pools. Each of  
106 the pools varies in space, time and over the twelve Plant Functional Types (PFTs). An extra PFT is used to represent bare  
107 soil. Natural and anthropogenic disturbances to the C pools include fire, crop harvest, changes to GPP, litterfall, autotrophic  
108 and heterotrophic respiration as a result of climatic changes (Krinner et al., 2005; Guimberteau et al., 2018). The C-cycle  
109 processes are represented by a C emulator that reproduces for each PFT all C pools and fluxes between the pools exactly as  
110 in ORCHIDEE in absence of erosion. A net land use change scheme is included in the emulator with mass-conservative  
111 bookkeeping of SOC and C input when a PFT is changed into another from anthropogenic land use change (Naipal et al.,  
112 2018). The sediment budget model has been added in the emulator to simulate large-scale long-term soil and SOC  
113 redistribution by water erosion using coarse-resolution precipitation, land-cover and LAI data from Earth System Models  
114 (Naipal et al. 2015, 2016). The C emulator including erosion removal was developed by Naipal et al. (2018) to reproduce  
115 SOC vertical profile, removal of soil and SOC starting from the topsoil, and compensatory SOC storage from litter input.  
116 As soil erosion is assumed not to change soil and hydraulic parameters but only the SOC dynamics, the emulator allows  
117 substituting for the ORCHIDEE model and performing simulations on time scales of millennia with a daily time step,  
118 which would be a very computationally expensive or nearly impossible with the full LSM. The concept and all equations of  
119 the emulator are described in Naipal et al. (2018). The following subsections describe the different components of the  
120 CE-DYNAM that couples the C and soil removal scheme (Naipal et al., 2018) with the horizontal transport and burial of  
121 eroded soil and C (Naipal et al., 2016).

122

## 123 **2.2 The soil erosion scheme**

124

125 The potential gross soil erosion rates are calculated by the Adjusted Revised Universal Soil Loss Equation (Adj. RUSLE)  
126 model (Naipal et al., 2015), which is part of the sediment budget model (Fig 1). In the Adj. RUSLE the yearly average soil  
127 erosion rate is a product of rainfall erosivity ( $R$ ), slope steepness ( $S$ ), land cover and management ( $Cm$ ) and soil erodibility  
128 ( $K$ ):

129

$$130 \quad E = S * R * K * Cm \quad (1)$$

131

132 The slope-length ( $L$ ) and support practice ( $P$ ) factors, which are part of the original Revised Universal Soil Loss Equation  
133 (RUSLE) model (Renard et al., 1997), have been excluded here because their quantification still includes many  
134 uncertainties and is not practical for applications at regional to global scales. These factors are a function of local manmade  
135 structures and management practices which are difficult to assess for present day and whose changes over the past are even  
136 more uncertain. In addition, we focus in this study on potential soil erosion and do not consider erosion-control practices.  
137 Naipal et al. (2015) have developed a methodology to derive the slope factor  $S$  and the erosivity factor  $R$  from 5 arcmin  
138 resolution (5 x 5 arcminute raster) data on elevation and precipitation, hereby preserving the high-resolution spatial  
139 variability in slope and temporal variability in erosivity. In the rest of the manuscript we will refer to  $X$  by  $X$  km/arcminute

140 raster cells always with X km/arcmin resolution. Despite the comparatively coarse resolution of the erosion model, the so  
 141 derived  $R$  factor was shown to compare well with the corresponding high-resolution product published by Panagos et al.  
 142 (2017). In the study of Naipal et al. (2016), where the soil erosion model was applied for the last millennium, the change in  
 143 climate was taken into account in the calculation of the  $R$  factor. For this study, we assume that the climate zones as defined  
 144 by the Koeppen-Geiger climate classification have not changed drastically since 1850 AD.

145

### 146 **2.3 The sediment deposition and transport scheme**

147

148 The sediment deposition and transport scheme have been adapted from the sediment budget model described by Naipal et  
 149 al. (2016), which has been calibrated and validated for the Rhine catchment (Fig 1). In the sediment budget model each  
 150 grid cell contains a floodplain fraction, which is needed to ensure sediment transport between the grid cells (transport from  
 151 one grid cell to another can only follow the connectivity of floodplains). It should be noted that global soil databases do not  
 152 identify floodplain soil as a separate soil class, although national soil databases might. However, the aim of this study is to  
 153 present a carbon erosion model that should be also applicable for other catchments and eventually, globally. Therefore, we  
 154 followed a two-step methodology to derive floodplains in the Rhine catchment using hydrological parameters and existing  
 155 data on hillslopes and valleys. First, grid cells were identified that consisted entirely out of floodplains. For this we used  
 156 the gridded global data set of soil at 5 arcminute resolution, with intact regolith, and sedimentary deposit thicknesses of  
 157 Pelletier et al. (2016) (Table 1), and identified lowlands and hillslopes based on soil thickness and depth to bedrock. The  
 158 lowlands were classified as grid cells that contain only floodplains and no hillslopes. Second, we calculated the floodplain  
 159 fraction ( $A_{fl}$ ) of a grid cell  $i$  that has both hillslopes and floodplains as a function of stream length and width based on the  
 160 methodology developed by Hoffmann et al. (2007):

161

$$162 \quad A_{fl}(i) = L_{stream}(i) * W_{stream}(i) \quad (2)$$

163

164 Where,  $L_{stream}$  is the stream length derived from the HydroSHEDS database (Lehner and Grill, 2013) (Table 1).

165

$$166 \quad W_{stream}(i) = a * A_{upstream}^b(i) \quad (3)$$

167

168 Where,  $A_{upstream}$  is the upstream catchment area, and  $a$  is equal to 60.8, and  $b$  is equal to 0.3.

169

170 The parameters  $a$  and  $b$  have been derived from the scaling behavior of floodplain width as estimated from measurements  
 171 on the Rhine (Hoffmann et al., 2007). The sediment deposition on hillslopes ( $D_{hs}$ ) and floodplains ( $D_{fl}$ ) is calculated as a  
 172 function of the gross soil removal rates ( $E$ ) according to Naipal et al. (2016) with the following equations:

173

$$174 \quad D_{fl}(i) = f(i) * E(i) \quad (4a)$$

175  
176  
177  
178  
179  
180  
181  
182  
183  
184  
185  
186  
187  
188  
189  
190  
191  
192  
193  
194  
195  
196  
197  
198  
199  
200  
201  
202  
203  
204  
205  
206  
207  
208  
209

$$D_{hs}(i) = (1 - f(i)) * E(i) \tag{4b}$$

$$f(i) = a_f * e^{\left(\frac{b_f * \theta(i)}{\theta_{max}}\right)} \tag{5}$$

Where,  $f$  is the floodplain deposition factor at 8 km resolution that determines the fraction of gross eroded material transported and deposited in the floodplain fraction of a grid cell.  $a_f$  and  $b_f$  are constant parameters that relate  $f$  to the average topographical slope ( $\theta$ ) of a grid cell depending on the type of land cover.  $\theta_{max}$  is the maximum topographical slope of the entire Rhine catchment.

The parameters  $a_f$  and  $b_f$  are chosen in such a way that  $f$  varies between 0.2 and 0.5 for cropland, reflecting the decreased sediment connectivity between hillslopes and floodplains created by man made structures such as ditches and hedges. For natural vegetation such as forests and natural grassland,  $a_f$  and  $b_f$  are chosen in a way that  $f$  varies between 0.5 and 0.8 assuming that in these landscapes hillslopes and floodplains are well-connected. This assumption on the reduced sediment connectivity for agricultural landscapes is supported by several previous studies (Hoffmann et al., 2013; de Moor and Verstraeten, 2008; Gumiere et al., 2011; Wang et al., 2015) on the effect of erosion on sediment yield. These studies show that man-made activities on agricultural landscapes result in a trapping of eroded soil in colluvial deposition sites, reducing the sediment transport from hillslopes to floodplains. The model parameter  $f$  has been calibrated for the Rhine catchment before in Naipal et al. (2016), where the ranges mentioned above are found to produce a ratio between hillslope and floodplain sediment storage that was comparable to observations. The studies of Wang et al. (2010; 2015) identify a range for the hillslope sediment delivery to be between 50 and 80 %, which is similar to the range in the (1-f) factor in our model. In each case and within the defined boundaries, the slope gradient determines the final value of  $f$ . Eroded material that has not been deposited in the floodplains stays on the hillslopes and is assumed to be deposited at the foot of the hillslopes as colluvial sediment.

The floodplain fractions of the grid cells are connected through an 8 km resolution flow routing network (Naipal et al., 2016), where the rivers and streams are indirectly included in the floodplain area but not explicitly simulated. By routing the sediment and C through the floodplain fractions of grid cells we lump together the slow process of riverbank erosion by river dynamics (time scale  $\approx$  a few years to thousands of years), and the rather fast process of transport of eroded material by the rivers (time scale  $\approx$  days). The rate by which sediment and SOC leave the floodplain of a grid cell to go to the floodplain of an adjacent grid cell is determined by the sediment residence time. The sediment residence time ( $\tau$ ) is a function of the upstream contributing area ( $Flowacc$ ):

$$\tau(i) = e^{\frac{Flowacc(i) - a_\tau}{b_\tau}} \tag{6}$$

210 The study of Hoffmann et al. (2008) shows that the majority of floodplain sediments have a residence time that ranges  
 211 between 0 and 2000 years, with a median of 50 years. The constants  $a_\tau$  and  $b_\tau$  are chosen in such a way that basin  $\tau$  varies  
 212 between the 5th and 95th percentile of those observations, with a median for the whole catchment of 50 years. These  
 213 constants are uniform for the whole basin. Floodplain C storage follows the same residence time as sediment on top of the  
 214 actual decomposition rate of C in a grid cell of ORCHIDEE. The routing of sediment and C between the grid cells follows  
 215 a multiple-flow routing scheme. In this scheme the flow coming from a certain grid cell is distributed across all lower-lying  
 216 neighbors based on a weight ( $W$ , dimensionless) that is calculated as a function of the contour length ( $c$ ):

$$218 \quad W_{(i+k,j+l)} = \frac{\theta_{(i+k,j+l)} * C_{(i+k,j+l)}}{\sum_{k,l=-1}^{k,l=1} [\theta_{(i+k,j+l)} * C_{(i+k,j+l)}]} \quad (7)$$

219  
 220 Where  $c$  is  $0.5 * \text{grid size (m)}$  in the cardinal direction and  $0.354 * \text{grid size (m)}$  in the diagonal direction.  $(i, j)$  is the grid cell  
 221 in consideration where  $i$  counts grid cells in the latitude direction and  $j$  in the longitude direction.  $i+k$  and  $j+l$  specify the  
 222 neighboring grid cell where  $k$  and  $l$  can be either  $-1, 0$  or  $1$ .  $\theta$  is calculated as the division between the difference in  
 223 elevation ( $h$ ) give in meters difference and the grid cell size ( $d$ ), also in meters:

$$225 \quad \theta_{(i+k,j+l)} = \frac{h_{(i,j)} - h_{(i+k,j+l)}}{d} \quad (8)$$

226  
 227 The sediment and C routing is done continuously at a daily time-step to preserve numerical stability of the model. More  
 228 detailed explanation of the methods presented in this section can be found in the study of Naipal et al. (2016).

## 230 **2.4 Litter dynamics**

231  
 232 The four litter pools in the emulator are an below- and an above- ground litter pool, each split into a metabolic and  
 233 structural pool with different turnover rates as implemented in ORCHIDEE (Krinner et al., 2005). The belowground litter  
 234 pools consist mostly out of root residues. Both the biomass and litter pools have a loss flux due to fire as incorporated in  
 235 ORCHIDEE by the Spitfire model of Thonicke et al. (2010). The litter that is not respired or burnt is transferred to the SOC  
 236 pools based on the Century model (Parton et al., 1987) and the vertical discretization scheme SOC scheme presented by  
 237 Naipal et al., (2018).

238  
 239 The vertical discretization scheme was introduced in the emulator to account for a declining C input and SOC respiration  
 240 with depth, and consists of 20 layers with each 10 cm thickness. The litter to soil fluxes from above-ground litter pools are  
 241 all attributed to the top 10 cm of the soil profile. The litter to soil fluxes from belowground litter pools are distributed  
 242 exponentially over the whole soil profile according to:

243

$$I_{be}(z) = I_{0be} * e^{-r*z} \quad (9)$$

Where  $I_{0be}$  is the below-ground litter input to the surface soil layer and  $r$  is the PFT-specific vertical root-density attenuation coefficient as used in ORCHIDEE. The sum of all layer-dependent litter to soil fractions is equal to the total litter to soil flux as calculated by ORCHIDEE. The vertical SOC profile is modified by erosion and the resulting deposition fluxes, which is discussed in detail in the following sections.

## 2.5 Crop harvest and yield

We adjusted the representation of crop harvest from ORCHIDEE by assuming a variable harvest index for C3 plants that increases during the historical period as shown in the study of Hay (1995) for Wheat and Barley, which are also the main C3 crops in the Rhine catchment. The harvest index is defined by the ratio of harvested grain biomass to above-ground dry matter production (Krunner et al., 2005). In this study the harvest index increases linearly between 0.26 and 0.46 (Naipal et al. 2018) consistent with the average values of Hay (1995). We also found that in certain cases the cropland NPP was too high during the entire period of 1850-2005, especially in the early part of the 20<sup>th</sup> Century. This is because the cropland photosynthetic rates were adjusted in ORCHIDEE to give a cropland NPP representative of present day values that are higher than for the low input agriculture of the early 20<sup>th</sup> Century. To derive a more realistic NPP for crop and barley in the Rhine catchment we used the long-term crop yield data obtained from a dataset on 120000 yield observations over the 20<sup>th</sup> century in Northeast French Départements (NUTS3 administrative division) (Schauberger et al., 2018). According to the yield data assembled by Schauberger et al. (2018), yields in Northeast France for these crops increased fourfold during the last century. Note that crop residues like straw constituted a larger fraction of the total biomass in 1850 than in 2005, but those residues were likely collected and used for animal feed, housing fuel. We did not account for this harvest of residue in the simulation of SOC.

## 2.6 SOC dynamics without erosion

The change in the carbon content of the PFT-specific SOC pools in the emulator without soil erosion as described by Naipal et al. (2018) (Fig 1):

$$\frac{dSOC_a(t)}{dt} = lit_a(t) + k_{pa} * SOC_p(t) + k_{sa} * SOC_s(t) - (k_{ap} + k_{as} + k_{0a}) * SOC_a(t) \quad (10)$$

$$\frac{dSOC_s(t)}{dt} = lit_s(t) + k_{as} * SOC_a(t) - (k_{sa} + k_{sp} + k_{0s}) * SOC_s(t) \quad (11)$$

$$\frac{dSOC_p(t)}{dt} = k_{ap} * SOC_a(t) + k_{sp} * SOC_s(t) - (k_{pa} + k_{0p}) * SOC_p(t) \quad (12)$$



279 Where,  $SOC_a$ ,  $SOC_s$ , and  $SOC_p$  ( $\text{g C m}^{-2}$ ) are the active, slow and passive SOC, respectively. The distinction of these SOC  
 280 pools, defined by their residence times, are based on the study of Parton *et al.* (1987). The active SOC pool has the lowest  
 281 residence time (1 - 5 years) and the passive the highest (200-1500 years).  $lit_a$  and  $lit_s$  ( $\text{g C m}^{-2} \text{ day}^{-1}$ ) are the daily litter  
 282 input rates to the active and slow SOC pools, respectively;  $kO_a$ ,  $kO_s$  and  $kO_p$  ( $\text{day}^{-1}$ ) are the respiration rates of the active,  
 283 slow and passive pools, respectively;  $k_{as}$ ,  $k_{ap}$ ,  $k_{pa}$ ,  $k_{sa}$ ,  $k_{sp}$  are the coefficients determining the flux from the active to the  
 284 slow pool, from the active to the passive pool, from the passive to the active pool, from the slow to the active pool and  
 285 from the slow to the passive pool, respectively.

286  
 287 The vertical C discretization scheme in the emulator assumes that the SOC respiration rates decrease exponentially with  
 288 depth:

$$290 \quad k_i(z) = k_{0i}(z) * e^{-re*z} \quad (13)$$

291  
 292 Where  $k_i$  is the respiration rate at a soil depth  $z$  and  $re$  ( $\text{m}^{-1}$ ) is a coefficient representing the impact of external factors, such  
 293 as oxygen availability that decreases with depth.  $k_0$  is the respiration rate of the surface soil layer for a certain SOC pool  $i$ .  
 294 The variable  $re$  is determined in such a way that the total soil respiration of a certain pool over the entire soil profile  
 295 without erosion is similar to the output of the full ORCHIDEE model. Detailed description of how this is done can be  
 296 found in the study of Naipal *et al.* (2018).

## 298 **2.7 C erosion on hillslopes**

299  
 300 In the model we assume that soil erosion takes place on hillslopes, and not in the floodplains due to the usually low  
 301 topographical slope of floodplains. The factor  $(1-f)$  determines the fraction of the eroded soil that is deposited in the  
 302 colluvial reservoirs (Fig 1). Soil erosion always removes a fraction of the SOC stock in the upper soil layer depending on  
 303 the erosion rate and bulk density of the soil. The next soil layer contains less C and therefore at the following time-step less  
 304 C will be eroded under the same erosion rate. To account for this effect, the SOC profile evolution is dynamically tracked  
 305 in the model and updated at a daily time step, conform with the method of Wang *et al.* (2015). First, a fraction of the C  
 306 from each soil pool in proportion to the erosion height is removed from the surface layer. Then, at the same erosion rate,  
 307 SOC from the subsoil layer becomes the surface layer, maintaining the soil layer thickness in the vertical discretization  
 308 scheme. Similarly, the SOC from the subsoil later also moves upward one layer. The removal of C by erosion also triggers  
 309 a compensatory C sink due to the reduction in SOC respiration on eroding land. This compensatory C sink and reduced C  
 310 erosion over time will ultimately lead to an equilibrium state. The change in C content due to erosion of the PFT-specific  
 311 pools for hillslopes can be represented by the following equations:

$$312 \quad \frac{dSOC_{HSi}(z,t)}{dt} = k_E * SOC_{HSi}(z + 1, t) - k_E * SOC_{HSi}(z, t) \quad (14)$$

314  
 315 Where  $dSOC_{HSi}(z,t)$  is the change in hillslope SOC of a component pool  $i$  at a depth  $z$  and at time step  $t$ . The daily erosion  
 316 fraction  $k_E$  (dimensionless) is calculated as following:

$$317 \quad k_E = \frac{f * \left(\frac{F}{365}\right)}{BD * dz} * EF \quad (15)$$

318  
 319  
 320 Where,  $E$  is the erosion rate ( $t \text{ ha}^2 \text{ year}^{-1}$ ),  $f$  is the floodplain deposition factor,  $BD$  is the average bulk density of the soil  
 321 profile ( $\text{g cm}^{-3}$ ),  $dz$  is the soil thickness ( $=0.1 \text{ m}$ ), and  $EF$  is the C enrichment factor that is set to 1 by default.  $EF > 1$   
 322 represents a higher C concentration in eroded soil compared to the original soil, due to the selectivity of erosion.

323  
 324 This part of the model has been already applied at the global scale as the C removal model presented by Naipal et al.  
 325 (2018) and is here extended with the deposition term detailed above.

## 326 327 **2.8 C deposition and transport in floodplains**

328  
 329 The SOC profile dynamics of floodplains are controlled by: (1) C input from the hillslopes, (2) C import by lateral  
 330 transport from the floodplain fractions of upstream neighboring grid cells, and (3) C export to the floodplain fractions of  
 331 downstream neighboring grid cells (Fig 1). First, the net eroded flux from the surface layer of the hillslope fraction of the  
 332 grid cell ( $k_E * SOC_{HS}(z=0)$ ) is incorporated in the surface layer of the floodplain. At the same deposition rate, the SOC of  
 333 the surface layer of the floodplain is incorporated in the subsoil layer. Similarly, a fraction of the SOC of the subsoil layer  
 334 is moved downward one layer. We will refer to this process as the ‘downward’ moving of C in the soil layer profile. It  
 335 should be noted that C selectivity during transport and deposition is not taken into account here, meaning that the C pools  
 336 of the deposited material are the same as the eroded material from the topsoil of eroding areas. At the same time a fraction  
 337 of the C of the surface layer proportional to the sediment residence time ( $\tau$ ) is exported out of the catchment following the  
 338 sediment routing scheme, resulting in the ‘upward’ moving of the C from the subsoil layers. This process represents the  
 339 river bank erosion and resulting POC export by rivers. It should be noted that rivers and streams are not explicitly  
 340 represented in the model. As we do not have information on the sub-grid spatial distribution of land cover fractions we first  
 341 sum the exported C flux over all PFTs before assigning the flux proportionally to the land cover fractions of the receiving  
 342 downstream-lying grid cells. The C that is imported from the neighboring grid cells follows the same procedure as the  
 343 deposition of eroded material, and results in a ‘downward’ moving of the C in the soil profile. The change in C content due  
 344 to deposition and river export/import of the PFT-specific pools for floodplains can be represented by the following  
 345 equations:

$$346 \quad \frac{dSOC_{FLi}(z,t)}{dt} = \left( (k_D + k_{i_{out}}) * SOC_{FLi}(z-1, t) \right) + \left( \frac{1}{(\tau * 365)} * SOC_{FLi}(z+1, t) \right) - \left( \left( k_D + \frac{1}{(\tau * 365)} + k_{i_{out}} \right) * SOC_{FLi}(z, t) \right), \text{ for}$$

347  
 348  $z > 0$  (16)

349

$$350 \quad \frac{dSOC_{FLi}(0,t)}{dt} = \sum_{n=1}^{n=9} \left( k_{i_{out}}(n) * SOC_{FLi}(0,t)(n) \right) + (k_E * SOC_{HSi}(0,t)) + \left( \frac{1}{(\tau*365)} * SOC_{FLi}(1,t) \right) - \left( \left( k_D + \frac{1}{(\tau*365)} + k_{i_{out}} \right) * SOC_{FLi}(0,t) \right)$$

351 , for z=0 (17)

352

353 Where  $n$  is the neighboring grid cell that flows into the current grid cell,  $dSOC_{FLi}(z,t)$  is the change in floodplain SOC of a  
 354 component pool  $i$  at a depth  $z$  and at time step  $t$ , and  $SOC_{HS}$  is the hillslope SOC stock.  $k_D$  is the deposition rate and equal  
 355 to:

356

$$357 \quad k_D = \frac{k_E * AREA_{HS}}{AREA_{FL}} \quad (18)$$

358

359 Where  $AREA_{HS}$  is the hillslope area and  $AREA_{FL}$  is the floodplain area ( $m^2$ ).  $k_{i_{out}}$  is the import rate per C pool  $i$  from  
 360 neighboring grid cells (dimensionless) and can be calculated as:

361

$$362 \quad k_{i_{out}} = \frac{\sum_{n=1}^{n=9} (W * \frac{1}{\tau*365} * AREA_{FL})(n)}{AREA_{FL}} \quad (19)$$

363

364 Where,  $W$  is the weight index of equation 7.

365

366 The first term of equation 16 represents the ‘downward’ moving of the incoming C related to the C deposition flux from  
 367 the hillslope fraction of the gridcell and the lateral C import flux from the floodplain fractions of upstream neighboring grid  
 368 cells. The second term represents the ‘upward’ moving of SOC related to the lateral C transfer to downstream neighboring  
 369 grid cells. The third term of equation 16 represents the total C loss flux from the current soil layer  $z$ , which is a result of  
 370 either the ‘upward’ or ‘downward’ moving of the C in the soil profile. The first term of equation 17 represents the  
 371 incoming lateral C flux from the floodplains of the upstream neighboring grid cells. The second term  
 372 represent the C deposition flux coming from the hillslope fraction of the grid cell. The third term represents the ‘upward’  
 373 moving of the SOC from the subsoil layer to the topsoil layer as a result of sediment/C routing. The last term of equation  
 374 17 represents the total loss of C from the topsoil layer, of which part is distributed across the neighboring grid cells  
 375 downstream ( $\frac{1}{(\tau*365)}$ ), and another part if moved ‘downwards’ in the soil profile as a result of C deposition ( $k_D$ ) and  
 376 the incoming later C from upstream grid cells ( $k_{i_{out}}$ ).

377

## 378 2.9 The land use change bookkeeping model

379

380 The land use change bookkeeping scheme includes the yearly changes in forest, grassland and cropland areas in each grid  
381 cell as reconstructed by Peng et al. (2017) (Table 1). Peng et al. (2017) derived historical changes in PFT fractions based on  
382 LUHv2 land use dataset (Hurtt et al., 2011), historical forest area data from Houghton, and present day forest area from  
383 ESA CCI satellite land cover (European Space Agency, ESA, 2014). By using different transition rules and independent  
384 forest data to constrain the changes in crop and urban PFTs he derived the most suitable historical PFT maps.

385  
386 When land use change takes place, the litter and SOC pools of all shrinking PFTs are summed and allocated proportionally  
387 to the expanding PFTs, maintaining the mass-balance. In this way the litter pools and SOC stocks get impacted by different  
388 input and respiration rates for each soil layer. When forest is reduced, three wood products with decay rates of 1, 10 and  
389 100 years are formed and harvested. The biomass pools of other shrinking land cover types are transformed to litter and  
390 allocated to the expanding PFTs. For more details on the land use scheme see the study of Naipal et al. (2018).

## 391 392 **2.10 Study-Area**

393  
394 The model is tested for the Rhine catchment (Fig 2), which has a total basin area of 185,000 km<sup>2</sup> covering five different  
395 countries in Central Europe. Its large size is beneficial for the application of a coarse-resolution model such as  
396 CE-DYNAM to study large-scale regional dynamics in the C cycle due to soil erosion. The Rhine catchment has a very  
397 interesting topography, with steep slopes larger than 20% upstream in the Alps, and large, wide and flat floodplains at the  
398 foot of the Alps, the upper Rhine and the lower Rhine. The floodplains store large amounts of sediment and C that  
399 originally was eroded from the steep hillslopes upstream. This makes it possible to study the long-term effect of erosion on  
400 hillslope and floodplain dynamics. Furthermore, the Rhine catchment has been experiencing different stages of land use  
401 change over the Holocene, with land degradation dating back to more than 5500 years ago (Dotterweich, 2013). In contrast,  
402 during the last two decades there has been a general afforestation and soil erosion has been decreasing. These land use  
403 changes and changes in erosion make an interesting and important case to study the effect of anthropogenic activities on  
404 the C cycle in Europe.

405  
406 In addition, the Rhine catchment has been the focus of many erosion studies providing observations on erosion and  
407 sediment dynamics that can be used for model validation (Asselman, 1999; Asselman et al., 2003; Erkens, 2009; Hoffmann  
408 et al., 2007, 2008, 2013a, 2013b; Naipal et al., 2016). The global sediment budget model that forms the basis for the  
409 sediment dynamics of CE-DYNAM has been validated and calibrated for the Rhine catchment with observations on  
410 sediment storage from Hoffmann et al. (2013) and the derived scaling relationships between sediment storage and basin  
411 area (Naipal et al., 2016). Hoffmann et al. (2008, 2013) did an inventory of 41 hillslope and 36 floodplain sediment and  
412 SOC deposits related to soil erosion over the last 7500 years. The floodplain sediment observations consist mostly out of  
413 organic material (gyttja, peat) and fine sediments (fine sand, loam, silt) in overbank deposits (Hoffmann et al., 2008). These  
414 fine sediments are a result of long-term soil erosion on the hillslopes. Hoffmann et al. (2013) found that the sediment and

415 SOC deposits were quantitatively related to the basin size according to certain scaling functions, where floodplain deposits  
416 increased in a non-linear way with basin size while the hillslope deposits showed a linear increase with basin size. We will  
417 use these relationships to validate the spatial variability in SOC storage of floodplains and hillslopes simulated by  
418 CE-DYNAM. The scaling relationships have the form of a simple power law:

$$419$$
$$420 M = a * \left(\frac{A}{A_{ref}}\right)^b \quad (20)$$
$$421$$

422 Where  $M$  is the sediment storage or the SOC storage,  $a$  is the storage (Mt) related to an arbitrary chosen area  $A_{ref}$ , while  $b$  is  
423 the scaling exponent.

424

## 425 **2.11 Input data and model simulations**

426

427 To create the C emulator that forms the underlying C cycle part of CE-DYNAM, we first ran the full ORCHIDEE model  
428 for the period 1850-2005 at a coarse resolution of 2.5°degrees latitude and 3.75° degrees longitude, and output all C pools  
429 and fluxes. The pools and fluxes were then archived together and used to derive the turnover rates to build the emulator.  
430 The SOC scheme of the emulator that has been modified to account for soil erosion processes has been made to run at a  
431 spatial resolution of 5 arcmin, similar to the original global sediment budget model. Then, we performed three main  
432 simulations with CE-DYNAM for the Rhine catchment. Simulation S0: The baseline simulation or no-erosion simulation,  
433 where SOC dynamics are similar to the full ORCHIDEE model. Simulation S1: The erosion -only simulation, where the  
434 hillslopes erode and all eroded C is respired to the atmosphere without reaching the colluvial and alluvial deposition sites.  
435 Simulation S2: The simulation with full sediment dynamics where hillslopes and floodplains are connected and can bury or  
436 loose C. We ran the emulator for 3000 years at a daily time step with the initial climate and land cover of the period  
437 1850-1860. To speed up the spin-up simulations we calculated the temporary equilibrium state of the floodplain SOC pools  
438 every 10 years analytically. At the end of the spin-up period the floodplain SOC pools were close to equilibrium, with a  
439 yearly change of less than 0.001% of the total floodplain SOC stock. Afterwards, we performed the transient simulations  
440 for the period 1851-2005 at a daily time step with changing climate and land cover conditions, using the equilibrium SOC  
441 stocks as baseline. To ensure a faster performance of CE-DYNAM we delineated the Rhine catchment in seven large  
442 sub-basins based on the flow direction and ran the model in parallel for each of the sub-basins at a daily timestep. After  
443 each year the sub-catchments exchanged the lateral C fluxes with each other.

444

445 We also performed seven additional sensitivity simulations and four additional uncertainty simulations. Simulation S1\_EF  
446 and S2\_EF are performed to test the model assumption of a C enrichment during erosion. Here, we changed the enrichment  
447 factor EF to two, based on the study of Lugato et al. (2018). Simulations S2\_Tmin and S2\_Tmax are performed to test the  
448 rate of C transport between floodplains. Here we modified the average sediment residence time for the Rhine catchment to  
449 a minimum of 60 years (50 % lower than the current value), and to a maximum of 128 years (50% higher than the current

450 value), respectively. However, we kept the maximum sediment residence time at 1500 years. Simulations S0\_RM, S1\_RM  
451 and S2\_RM are performed to test the model assumption on crop residue management, where we assumed that all  
452 above-ground crop litter is harvested.

453  
454 For the uncertainty analysis we performed simulations S1\_min and S2\_min based on a minimum soil erosion scenario, and  
455 S1\_max and S2\_max based a maximum soil erosion scenario. These soil erosion scenarios are based on the uncertainty  
456 ranges in the rainfall erosivity and land cover factors of the erosion model. All the model simulations are summarized in  
457 table 2.

458

## 459 **2.12 Validation methods and data**

460

461 We performed a detailed model validation of the sediment and the C part of the model based on the following steps: (1)  
462 validation of soil erosion rates using observational and high-resolution model estimates for Germany and Europe, (2)  
463 validation of C erosion rates using high-resolution model estimates for Europe from Lugato et al. (2018), (3) validation of  
464 the spatial variability of hillslope and floodplain C storage using observational results from Hoffmann et al. (2013), (4)  
465 validation of SOC stocks using observational data from a global soil database and a European land use survey.

466

467 The validation of the soil erosion module has been done before in the studies of Naipal et al. (2015, 2016). However, we do  
468 it again in this study due to different input datasets. For the validation of gross soil erosion rates we used the  
469 high-resolution model estimates from the study of Panagos et al. (2015), who applied the RUSLE2015 model at a 100 m  
470 resolution at European scale for the year 2010. The RUSLE2015 is derived from the original RUSLE model with some  
471 modifications to the model parameters L, C and P. The erosion module of CE-DYNAM is also based on a modified  
472 version of the RUSLE (Adj.RUSLE) which, however, lacks the L and P factors. It calculates the potential soil erosion rate  
473 under the assumption of no erosion control scenarios, in contrast to RUSLE2015, which does represent erosion control  
474 practices. Adj.RUSLE also differs from RUSLE2015 in the use of more coarsely resolved input datasets (table 1), for  
475 which the equations for the R and S factors have been modified. The extensive validation of the Adj. RUSLE model in this  
476 study and previous studies (Naipal et al., 2015, 2016, 2018), shows that despite its coarse resolution, the methodology  
477 works for large spatial scales. In contrast, RUSLE2015 uses largely similar equations as in the original RUSLE model  
478 presented in Renard et al. (1997). Thus, even though both Adj.RUSLE and RUSLE2015 are derived from the same erosion  
479 model, the differences between the models are large, and would justify our model comparison. Furthermore, we used  
480 independent high-resolution erosion estimates from the study of Cerdan et al. (2010), available at a 1 km resolution at  
481 European scale, which were based on an extensive database of measured erosion rates under natural rainfall in Europe. For  
482 the comparison we aggregated the high-resolution model results of both datasets to the resolution of CE-DYNAM. We  
483 also used the potential soil erosion map of the Federal Institute for Geosciences and Natural Resources of Germany (Bug  
484 and Stolz, 2014). This map presents the yearly average soil erosion rates at 250 m resolution on agricultural land derived

485 from a USLE-based approach, with some modifications to the erosion factors and input data. Before validating our model  
486 results we also aggregated these high-resolution erosion rates to the coarser resolution of our model.

487

488 Validation of our net soil erosion rates is done based on the 100 m resolution net soil erosion rates derived with the  
489 WATEM-SEDEM model (Borrelli et al., 2018). WATEM-SEDEM simulates soil removal by water erosion based on the  
490 USLE approach, sediment transport and deposition based on the transport capacity. The model has been extensively  
491 employed to estimate net fluxes of sediments across hillslopes at, catchment- and regional-scale level.

492

493 For the validation of C erosion rates, we used the high-resolution model results from Lugato et al. (2018), where they  
494 coupled the RUSLE2015 erosion model to the Century biogeochemistry model. These model results were available at a  
495 resolution of 1 km, where each gridcell was composed of an erosion and deposition fraction. The C erosion rates provided  
496 by Lugato et al. (2018) were multiplied with the erosion fraction of a 1 km grid cell. Then, the C erosion rates were  
497 aggregated to the resolution of CE-DYNAM. Lugato et al. (2018) provided an enhanced and a reduced erosion-induced C  
498 sink uncertainty scenario, based on different assumptions for C enrichment, burial and C mineralization during transport. In  
499 CE-DYNAM the C erosion rates from simulation S1 are multiplied with the hillslope area to get the total C erosion flux of  
500 a grid cell. As the study of Lugato et al. (2018) considers only agricultural areas, we considered only the crop fraction of a  
501 grid cell. It should be noted that the SOC dynamics scheme of CE-DYNAM, which is derived from ORCHIDEE LSM, is  
502 based on the Century model. However, there are large differences between the Century model used by Lugato et al. (2018)  
503 and the C dynamics scheme of ORCHIDEE used in this study. For example, in the Century model the crop productivity is  
504 mediated by nitrogen availability, which is not the case in the ORCHIDEE version used for this study. The Century model  
505 also includes some management practices such as crop rotations, which are not represented in ORCHIDEE. The Century  
506 model runs at a much higher resolution and is calibrated for agricultural land, while ORCHIDEE also simulates forest,  
507 grasslands and bare soil. In this way, the final SOC stocks derived with CE-DYNAM are also a result of erosion from other  
508 land cover types and land use changes. This is an important feature for land use change, which is not included in the  
509 Century model. Furthermore, the ORCHIDEE LSM has been used in many global intercomparisons and extensively  
510 evaluated for C budgets (Mueller et al., 2019; Todd-Brown et al., 2013). Also an important advantage of ORCHIDEE is  
511 that it includes the last century change in crop production calibrated against data (Guenet et al., 2018).

512

513 For the validation of the spatial variability of the SOC stocks of hillslopes and floodplains we used the scaling relationships  
514 between basin area and SOC storage derived by Hoffmann et al. (2013). The study by Naipal et al. (2016) found that the  
515 global sediment budget model is able to reproduce the scaling parameters for sediment storage, and after analyzing the  
516 dependence of the scaling behavior on the main parameters of the model, they argue that the scaling is an emergent feature  
517 of the model and mainly dependent on the underlying topography. This indicates that the scaling features of floodplain and  
518 hillslope sediment and C storage should also be applicable to the more recent time period, such as in our study. In our study  
519 we aim to evaluate the ability of CE-DYNAM to reproduce this scaling behavior for the SOC storage of the Rhine. For this  
520 purpose we selected the grid cells that contained the points of observation of the study of Hoffmann et al. (2013) and

521 performed a regression of the basin area (defined as the upstream contributing area) and the SOC storage of that gridcell  
522 for floodplains and hillslopes separately. Comparing the absolute values of the sediment and SOC storages of each grid cell  
523 from Hoffmann et al. (2013) was not possible due to the difference in the time-period of the studies, where Hoffmann et al.  
524 (2013) focussed on the entire Holocene, while our study focussed only on the period from 1850 AD.

525  
526 For the validation of the total SOC stocks we used the Global Dataset for Earth System Modeling (GSDE) (Shangguan et  
527 al., 2014) available at a spatial resolution of 1km and the Land Use/Land Cover Area Frame Survey (LUCAS) (Palmieri et  
528 al., 2011). The LUCAS topsoil SOC stocks, available at a high spatial resolution of 500 m, were calculated using the  
529 LUCAS SOC content for Europe (de Brogniez et al., 2015) and soil bulk density derived from soil texture datasets  
530 (Ballabio et al., 2016).

### 531 532 **3 Results**

533  
534 Due to large uncertainties in the model and validation data for the Alpine region we only present and discuss the model and  
535 validation results for the non-Alpine part of the Rhine catchment.

#### 536 537 **3.1 Model validation**

538 In this section we present the model validation results using the methods and validation data described in detail in the  
539 previous section.

540  
541 We find that the quantile distribution of the simulated gross soil erosion rates compares well to the distributions of other  
542 observational and high-resolution modelling studies (Cerdan et al., 2010, Panagos et al., 2015, Bug et al., 2014) (Fig 3A,  
543 B, C). It should be noted that our study, the study of Cerdan et al. (2010) and Bug et al. (2014) simulated potential soil  
544 erosion rates, not accounting for erosion control practices that are captured by the P-factor. We also find that the quantile  
545 distribution of the simulated net soil erosion from hillslopes in our study compares well with the distribution from the  
546 high-resolution modelling study of Borrelli et al. (2018) (Fig 3D). Furthermore, we performed a spatial comparison of our  
547 simulated gross and net erosion rates to those of the studies mentioned above. For this purpose we delineated 13 sub-basins  
548 in the Rhine catchment (Fig S3). Table 3 summarizes the resulting goodness-of-fit statistics of this comparison and shows  
549 that our erosion model is generally in good agreement with the other studies at sub-basin level.

550  
551 We find that the quantile distributions of our simulated agricultural carbon erosion and deposition rates are similar to those  
552 of the high-resolution modelling study of Lugato et al. (2018) (Fig 4A-D). Also the spatial variability of the C erosion rates  
553 at sub-basin level is in good comparison to the validation data (table 4). However, the linear regression between soil  
554 erosion and C erosion rates of our study lies at the lower end of the relationships derived from the enhanced and reduced  
555 erosion scenarios of Lugato et al. (2018) (Fig 5). This could be explained by the fact that we do not explicitly consider



556 erosion-control and management practices on agricultural land, and the coarse resolution of our model. The decreased  
557 spread in our simulated values is also a result of the coarse resolution of our model.

558  
559 Accounting for erosion, deposition and transport of SOC leads to a better representation of the simulated topsoil C stocks  
560 per land cover type when compared to SOC stocks of the LUCAS database (Fig 6). The simulated SOC stocks of the top  
561 20 cm of the soil profile fall within the quantile range of the LUCAS SOC stocks for cropland and forest (Fig 6). The  
562 topsoil SOC stocks for grassland improve but still show a large uncertainty range. Furthermore, we find that in both the  
563 erosion and no-erosion simulation the SOC stocks for grassland are higher than for forest. This is also observed in the  
564 study of Wiesmeier et al. (2012) in South-Germany where they found considerable higher SOC stocks for grassland with a  
565 median of 11.8 kg C m<sup>-2</sup> compared to forest based on the analysis of 1460 soil profiles. Furthermore, the comparison of the  
566 simulated total SOC stocks to those of the LUCAS and GSDE databases at sub-basin level shows a good model  
567 performance with respect to the spatial variability in topsoil SOC stocks (Table 5). To validate the spatial variability of  
568 floodplain and hillslope SOC stocks separately, we used the scaling relationships found by Hoffmann et al. (2013) (section  
569 2.12). We find a significantly larger exponent for the scaling relationship between the simulated floodplain SOC storage  
570 and basin area compared to the simulated hillslope SOC storage, when using the grid cells that contain the points of  
571 observation corresponding to the study of Hoffmann et al. (2013). This result is in line with what Hoffmann et al. (2013)  
572 found and shows that CE-DYNAM can realistically reproduce the spatial variability in SOC stocks between hillslopes and  
573 floodplains (table 6). However, when deriving the scaling relationships at sub-basin level instead of using individual grid  
574 cells we do not find a significant difference in scaling between floodplains and hillslopes (table 6).

### 575 576 **3.2 Model application**

577  
578 We find an average annual soil erosion rate of 1.44±0.82 t ha<sup>-1</sup> year<sup>-1</sup> over the period 1850-2005, which is about half of the  
579 average erosion rate simulated for the last millennium (Naipal et al., 2016) and falls into the range of the average erosion  
580 rate of the Holocene (Hoffmann et al., 2013). This soil erosion flux mobilized around 66±28 Tg of C over the period  
581 1850-2005, of which on average about 57% is deposited in colluvial reservoirs, 43% is deposited in alluvial reservoirs,  
582 while 0.2% is exported out of the catchment.

583  
584 The lower average annual soil erosion rate over the study period compared to the last millennium is a result of the general  
585 afforestation in the non-Alpine part of the Rhine catchment that started around 1910 AD (Fig 7B). Land cover data shows  
586 that forest increases by 24% over the period 1910-2005, mostly as a result of grassland to forest conversion. Cropland  
587 decreases by 6% over the period 1920 and 1970, and is relatively stable afterwards. This afforestation leads to a long-term  
588 decreasing trend in gross soil and SOC erosion rates on hillslopes (Fig 7C). The temporal variability in the soil and C  
589 erosion rates is a result of direct changes in precipitation, such as the temporary increase in erosion rates over the period  
590 1940-1960 (Fig 7A). Furthermore, we find that the temporal variability in C erosion rates follow the soil erosion rates

591 closely, indicating that soil erosion dominates the variations in C erosion over this time-period, while increased SOC stocks  
 592 due to CO<sub>2</sub> fertilization and afforestation play a secondary role as a slowly varying trend. It should be noted that the  
 593 correlation between soil and C erosion might be affected by processes not properly captured by the model such as the  
 594 selectivity of erosion, which also include the enrichment of C in eroded material.

595  
 596 The cumulative C erosion removal flux of 66±28 Tg of C leads to a cumulative net C sink for the whole Rhine region of  
 597 216±23 Tg C (Fig 7D). This is about 2.1 – 2.7 % of the cumulative NPP and of the same magnitude as the cumulative land  
 598 C sink of the Rhine without erosion. It should be noted that these are potential fluxes, assuming that the photosynthetic  
 599 replacement of C is not affected by the degradation of soil due to the removal of nutrients, declining water-holding capacity  
 600 and other negative changes to the soil structure and texture (processes not covered by our model). The breaking point in  
 601 figure 7D around 1910 AD is a result of the climate data used as input.

602  
 603 To better understand the erosion-induced net C flux, we analyze the erosion-induced C exchange with the atmosphere by  
 604 creating C budgets for the entire Rhine catchment for the period 1850-1860 and for the period 1950-2005 (Fig 8A&B).  
 605 These C budgets also shed light on changes in the linkage between lateral and vertical C fluxes over time. As we do not  
 606 explicitly track the movement of eroded C through all reservoirs (for example between eroding hillslopes and colluvial  
 607 reservoirs), we make use of the changes in SOC stocks and NEP of the three main simulations (S0, S1, S2) to derive the  
 608 erosion-induced vertical C fluxes. By subtracting the Net Ecosystem Productivity of hillslopes (NEP<sub>HS</sub>), which is the  
 609 difference between NPP and heterotrophic respiration, of the no-erosion simulation (S0) from the erosion-only simulation  
 610 (S1), we derive the additional photosynthetic replacement of SOC on eroding sites (Eq. 21):

$$611 \quad E_{rep} = NEP_{HS}(S1) - NEP_{HS}(S0) \quad (21)$$

612  
 613 Where,  $E_{rep}$  is the potential dynamic Photosynthetic replacement of C on eroding sites (assuming no feedback of erosion on  
 614 NPP). Part of the eroded C that is transported to and deposited in colluvial reservoirs can be respired or buried (Eq. 22).  
 615 The difference between NEP of simulation S2 and S1 is the NEP caused by the deposition of eroded C in colluvial areas  
 616 and equal to the difference between the burial and respiration of C in colluvial sites. As we do not explicitly track the  
 617 respiration of deposited material in the model, we can only derive the net respiration or net burial of colluvial deposits  
 618 ( $R_{C_{net}}$ ) with the following equation:

$$619 \quad R_{C_{net}} = NEP_{HS}(S2) - NEP_{HS}(S1) \quad (22)$$

620  
 621 The same concept can be applied for the net respiration of floodplains:

$$622 \quad R_{a_{net}} = NEP_{FL}(S2) - NEP_{FL}(S0) \quad (23)$$

626  
627 Where,  $NEP_{FL}$  is the floodplain Net Ecosystem Productivity, and  $Ra_{net}$  is the net respiration or net burial of alluvial  
628 deposits. Positive values for  $Ra_{net}$  or  $Rc_{net}$  indicate a net burial (respiration  $S2 <$  respiration  $S0/S1$ ) of the deposited  
629 material.

630  
631 We find that the dynamic replacement of C on eroding sites increased by 17-33% at the end of the period despite  
632 decreasing soil erosion rates (Fig 8A&B). This increase in the photosynthetic replacement of C is due to the globally  
633 increasing  $CO_2$  concentrations that lead to the  $CO_2$  fertilization effect, amplified by the afforestation trend in the Rhine over  
634 this period. Without this fertilization effect, soil erosion and deposition would be likely a weaker C sink or even a C source  
635 over the period 1850-2005 (Fig S4 A&B). This  $CO_2$  fertilization effect promotes a 100% replacement of the eroded C on  
636 hillslopes and even leads to a C sink on hillslopes at the end of the study period (Fig 8B). Furthermore, we find that the  
637 yearly average gross C erosion flux from eroding sites decreases by 10-34%, while the yearly deposition fluxes in colluvial  
638 and alluvial sites decreases by 20% and 19-47%, respectively. The decrease in the deposition flux to floodplains is  
639 compensated by a better sediment connectivity between hillslopes and floodplains due to afforestation. Forests have less  
640 man-made structures that can prevent the erosion fluxes from reaching the floodplains, which is represented by a higher  
641 floodplain deposition ' $f$ ' factor in the model. The decrease in the erosion flux also leads to a decreased POC export of the  
642 catchment at the end of the study period.

643  
644 We also find that both the colluvial and alluvial reservoirs show a net respiration flux throughout the time period (Fig  
645 8A&B). This is consistent with previous studies who found that deposition sites can be areas of increased  $CO_2$  emissions  
646 (Billings et al., 2019; Van Oost et al., 2012). However, there is a slight difference in the respiration of deposited C between  
647 the start and end of the transient period. The respiration of deposited SOC in colluvial sites increases with time while the  
648 respiration of deposited SOC in alluvial sites shows rather a decreasing trend. These changes in SOC respiration of  
649 deposited material depends on (1) the amount of deposited material, (2) increasing temperatures over 1850-2005 for the  
650 entire catchment, and (3) the constant removal of C-rich topsoil and its deposition in alluvial and colluvial reservoirs,  
651 which makes the deposited sediments generally richer in C than soils on erosion-neutral sites, providing more substrate for  
652 respiration. The largest increase in total respiration of alluvial and colluvial deposits takes place in hilly regions due to the  
653 initial increase in erosion rates resulting in large deposits of C. Overall, we find that the increased respiration of deposited  
654 material slightly offsets the increased dynamic C replacement, however, the dynamic C replacement on eroding sites still  
655 dominates the erosion-induced C sink.

#### 656 657 **4 Discussion**

658  
659 In this chapter we discuss some of the most important model limitations, uncertainties and assumptions.

660

#### 661 **4.1 Initial conditions and past global changes**

662  
663 Initial climate and land cover/use conditions needed to perform the equilibrium simulation together with the length of the  
664 transient period are essential parameters that determine the resulting spatial distribution of soil and C. Landscapes are in a  
665 constant transient state due to global changes, such as climate change, land use change, accelerated soil erosion. However,  
666 we assumed an equilibrium state so that we can quantify the changes during the transient period. The more one goes back  
667 in time to select the initial conditions and the longer the transient period that covers the essential historical environmental  
668 changes, the more accurate are the present-day distribution of SOC stocks, sediment storages, and related fluxes. This is  
669 especially true when analyzing the redistribution of soil and C as a result of erosion, deposition and transport, as these soil  
670 processes can be very slow. For example, the study of Naipal et al. (2016) shows that by simulating the soil erosion  
671 processes for the last millennium a spatial distribution of sediment storages that is similar to observations can be found. In  
672 this study we modeled steady state initial conditions of the period 1850-1860 due to constraints in data availability on  
673 precipitation and temperature, and because the aim of this study is to present the potential and limitations of the new model  
674 CE-DYNAM rather than provide precise values for soil and C stocks and fluxes. By focusing only on the period 1850-2005  
675 we miss the effects of significant land use changes in the past that coincided with times of strong precipitation such as in  
676 the 14<sup>th</sup> and 18<sup>th</sup> century. These major anthropogenic changes in the last Holocene substantially affected the present-day  
677 spatial distribution and size of SOC stocks.

678  
679 As a result, our model shows that floodplains store less SOC than hillslopes. However, we do find that floodplains have an  
680 overall higher C concentration ( $12 \text{ kg m}^{-2}$ ) compared to hillslopes ( $9 \text{ kg m}^{-2}$ ) at the end of the transient period (Fig 9A),  
681 which is in line with the findings of Hoffmann et al. (2013) and what can be derived from global soil databases. This is a  
682 result of higher SOC concentrations in deeper soil layers of floodplains compared to hillslopes (Fig 9 A & B). Although,  
683 the difference in C concentrations between floodplains and hillslopes is not as significant as is shown in the study of  
684 Hoffman et al. (2013). This is due to the absence of a higher local plant productivity resulting from favorable soil nutrient  
685 and hydrological conditions in our modelled floodplains.

#### 686 687 **4.2 Model advantages and limitations**

688  
689 Although we parameterized and applied CE-DYNAM for the Rhine catchment, it is intended to be made applicable to  
690 other large catchments globally. CE-DYNAM combines soil erosion processes, for which small scale differences in  
691 topography are of utter importance, with a state-of-the-art representation of large-scale SOC dynamics driven by land use  
692 and environmental factors (climate, atmospheric  $\text{CO}_2$ ) as simulated by the ORCHIDEE LSM. The flexible structure of  
693 CE-DYNAM makes the model adaptable to the SOC dynamics of other LSMs. In this way it is possible to study the main  
694 processes behind the linkages between soil erosion and the global C cycle.

695

696 CE-DYNAM explicitly accounts for hillslope and floodplains re-deposition, which is to our knowledge unique for a  
697 large-scale C erosion model and highly novel. However, it still lacks important processes affecting the C dynamics in  
698 floodplains. The model does not account for a slower respiration rate due to low-oxygen conditions, physical and chemical  
699 stabilization (Berhe et al., 2008; Martínez-mena et al., 2019) or a higher NPP for nutrient-rich floodplains (Van Oost et al.,  
700 2012; Hoffmann et al., 2013). The oxidation and preservation of C in deposition environments, especially in alluvial  
701 reservoirs remain highly uncertain (Billings et al., 2019).

702  
703 Due to its simplistic nature and coarse-resolution, CE-DYNAM does not resolve rivers and streams explicitly but assumes  
704 that they are included in the floodplain parts of the grid cells. CE-DYNAM has been developed and calibrated to simulate  
705 long-term changes in sediment and C storage on land and not the short-term variations in sediment and POC fluxes carried  
706 by rivers. This limits the application of CE-DYNAM in its current form to accurately quantify sediment and POC fluxes of  
707 rivers and streams. CE-DYNAM produces a sediment export flux at the end of the year 2005 of about  $1.6 \times 10^7$  tonnes per  
708 year, which is a magnitude higher than the measured suspended sediment flux of about  $3.15 \times 10^6$  tonnes per year (Asselman  
709 et al., 2003). The higher sediment flux is the result of absent riverine processes in CE-DYNAM such as river embankment,  
710 sediment burial behind dams, and the fact that we assume an equilibrium state for the Rhine catchment based on the period  
711 1850-1860 where agricultural soil erosion rates were already high. The simulated total cumulative sediment export of 2.5  
712 Gt for the Rhine over the period 1850-2005 is about 36 % of the cumulative gross soil erosion flux of 6.8 Gt. This sediment  
713 flux leads to a cumulative POC export of about 0.14 Tg of C for the Rhine over the period 1850-2005. This is 0.2 % of the  
714 cumulative C erosion flux. The yearly POC flux at the end of the year 2005 is  $0.02 \text{ tC km}^2 \text{ year}^{-1}$  (normalized over the  
715 total basin area), which is an order of magnitude lower compared to other studies who found a total POC export for the  
716 Rhine of about  $0.9 \text{ t C km}^2 \text{ year}^{-1}$  (Beusen et al., 2005; Sorribas et al., 2017). This underestimation in POC in  
717 CE-DYNAM is most likely a result of the high sediment residence time of floodplains downstream of the Rhine and the  
718 absence of increased plant productivity of floodplains, leading to the decomposition of a large fraction of the deposited C.  
719 Increased plant productivity of floodplains is shown to contribute significantly to the higher SOC stocks of floodplains  
720 compared to hillslopes, and to the export of DOC and POC to rivers (Van Oost et al., 2012; Hoffmann et al., 2013). In  
721 addition, the model lacks processes that account for the transformations between POC, DOC and  $\text{CO}_2$  and their fate in  
722 rivers and streams. The model also assumes a 'natural' state of the catchment where there is no river embankment and the  
723 floodplains are more or less dynamic. This may affect the behaviour of the POC export and residence time of C in  
724 floodplains.

725  
726 Furthermore, the model does not take into account the full effects of the selectivity of erosion, often expressed as the  
727 enrichment ratio, where the C content of eroding soil or the deposited sediment can be different from that of the original  
728 soil. The enrichment ratio can be very variable across landscapes, while the importance of erosion selectivity for C is still  
729 under debate (Nadeu et al., 2015; Wang et al., 2010). However, we did a simple sensitivity test to study the effect of C  
730 enrichment by erosion (section 4.3).

731

732 CE-DYNAM does not account for different ratios between the SOC pools (active, slow, passive) with depth due to the  
733 limitation in information to constrain these fractions for floodplains and hillslopes. However, this can be potentially  
734 important for respiration of C in depositional sites and during transport. Studies show that the labile C is decomposed first  
735 during sediment transport and directly after deposition, leaving behind the more recalcitrant C in deposition sites (Berhe et  
736 al., 2007; Billings et al., 2019). Due to the simplistic nature of our coarse-resolution model and the lack of data on  
737 oxidation of eroded C during transport we did not include C respiration during transport in the model.

738  
739 The current SOC scheme of CE-DYNAM does also not account for different residence times of SOC as a function of  
740 landscape position along a hillslope. The SOC decomposition rates can vary significantly along a hillslope due to changes  
741 in soil moisture, temperature, aggregation, and the transport of minerals and nutrients (Doetterl et al., 2016). Currently,  
742 these processes are not resolved in coarse resolution LSMs, contributing to the uncertainty in the large-scale linkage  
743 between soil erosion and SOC dynamics.

744  
745 Furthermore, there is no feedback between soil erosion and plant productivity in the model. To account for such process  
746 soil erosion processes would need to be explicitly included in an LSM such as ORCHIDEE, which would increase the  
747 computational complexity of the simulations substantially. The lack of this feedback results in an unlimited dynamic  
748 replacement of C on eroding sites.

749  
750 Currently, the erosion module of CE-DYNAM does not include the L (slope-length) and P (support-practice) factors. This  
751 might induce some bias in the results, especially for agricultural land. In our next study we aim to make CE-DYNAM  
752 better applicable for agricultural land, where these factors play an important role. For this purpose we will focus on the  
753 development of new methods that can quantify the L and P factors reliably at the global scale, and will need to re-calibrate  
754 the erosion module of CE-DYNAM, the Adj.RUSLE. Our decision of leaving out the L and P factors from the erosion  
755 equation in our study is based on the global study of Doetterl et al. (2012), which showed that the S, R, C and K factors  
756 explain approximately 78% of the total erosion rates on cropland in the USA. This indicates that on cropland the L and P  
757 factors, which are related to agriculture and land management, contribute only for 22 % to the overall erosion rates. This  
758 percentage is comparable to the uncertainty range in the estimation of the S, R, C and K factors at the regional scale from  
759 coarse resolution data. Renard and Ferreira (1993) also mention that the soil loss estimates are less sensitive to slope length  
760 than to most other factors. Furthermore, various studies argue that the estimation of the L factor for large areas is  
761 complicated and thus can induce significant uncertainty in soil erosion rates calculated based on coarse resolution data  
762 (Foster et al., 2002; Kinnell, 2007). Especially, for natural landscapes, such as forest, the estimation of the L factor is not  
763 straightforward as these natural landscapes usually include steep slopes (Elliot, 2004). In order to stay consistent with the  
764 estimation of potential soil erosion for all land cover types, we removed the L factor from the equation. The Adj.RUSLE  
765 has been already successfully validated at the regional scale, without the L and P factors where the spatial variability of soil  
766 erosion rates compares well to other high resolution modeling studies and observational data and the absolute values fall  
767 within the uncertainty ranges of those validation data (Naipal et al., 2015; Naipal et al., 2016; Naipal et al., 2018; and this

768 study). Finally, the aim of this study was to develop and validate a carbon erosion module for applications at the global  
769 scale, where the estimations of the L and P factors is even more limited. By showing that the erosion rates from the  
770 Adj.RUSLE and CE-DYNAM are within the uncertainty of other data and modelling studies, we can assume that it will be  
771 applicable for other large catchments in the temperate region.

772  
773 Finally, CE-DYNAM considers only the rather ‘slow’ rill and interrill soil erosion processes, and does not take into  
774 account gully erosion and landslides, which are bound to extreme precipitation events. The daily timestep of CE-DYNAM  
775 and the current setup of the sediment budget module allows only for long-term yearly average changes in erosion and  
776 deposition rates and cannot be applied to estimate episodic erosion and deposition events.

### 777 778 **4.3 Sensitivity analysis**

779  
780 We analyzed the effects of the following model assumptions: (1) C enrichment during erosion, (2) the floodplain sediment  
781 residence time, and (3) crop residue management.

782  
783 To test the C enrichment we increased the EF (Eq. 15) from 1 to 2, assuming a strong enrichment of C during erosion  
784 (section 2.11). We find that this enrichment results in a gross C erosion flux that is 1.61 times larger compared to the flux  
785 without enrichment (table 7). This leads also to a larger dynamic replacement of C on eroding sites in combination with a  
786 larger burial in depositional sites, which is in accordance with the study of Lugato et al. (2018). The resulting C sink from  
787 the enrichment simulation is 1.25 times larger than the sink under default conditions. However, we do not find a significant  
788 effect on the cumulative POC flux under C enrichment (table 7).

789  
790 To test the potential effects of a different sediment residence time on the SOC dynamics, we performed a sensitivity study  
791 where we changed the basin average sediment residence time to be 50% higher or 50% lower but keeping the maximum  
792 sediment residence time at 1500 years (section 2.11). By changing the average sediment residence time and keeping the  
793 maximum fixed, it will be the grid cells with the lowest residence times that will undergo the largest changes in residence  
794 time and consequently in the floodplain SOC storage and export. The higher the residence time, the longer the deposited  
795 soil C will reside in the floodplains, where it can either be respired or buried in deeper soil layers. Therefore, we find that  
796 the effects of the sediment residence time on the SOC dynamics are non-linear. Under default conditions we find the  
797 highest SOC storage. A 50% higher average sediment residence time leads to the lowest total SOC storage, with a decrease  
798 of 30% compared to default conditions, while the erosional C sink is reduced by 20% (table 7). This could be explained by  
799 a higher C decomposition flux for floodplains due to the long residence time of C in deposition areas. Especially, in  
800 mountainous regions where the soil erosion flux is large and removes a large part of the labile C, a higher sediment  
801 residence time will lead to higher C decomposition emissions in floodplains. The turnover seems to dominate over the C  
802 burial in deeper layers and export. A 50% lower average sediment residence time also leads to a decrease (of 8%) in the  
803 total SOC storage and a decrease of 6% in the erosional C sink compared to default conditions (Table 7). Also here, the

804 largest changes are found in mountainous regions where a low sediment residence time leads to a large export of C, which  
805 is then deposited in lower lying, more extensive floodplains. Thus, increasing or decreasing the residence time leads to a  
806 smaller total SOC storage, resulting from different spatial distributions of this SOC storage. The POC flux under the low  
807 sediment residence time scenario is substantially higher than under default conditions (table 7).

808  
809 To test the effects of crop residue management we harvest all above-ground crop residues (section 2.11). We find that total  
810 litter C stock is about 15% smaller compared to the default case by the end of the year 2005. This leads to a total change in  
811 the transient SOC stocks that is 20% smaller under no erosion (S0), and 26% smaller under erosion (S2) (table 7). Our  
812 findings confirm that soil management practices such as residue management have a substantial effect on the SOC  
813 dynamics.

814

## 815 **5 Conclusions**

816

817 We presented a novel spatially-explicit and process-based C erosion dynamics model, CE-DYNAM, which simulates the  
818 redistribution of soil and C over land as a result of water erosion and calculates the role of this redistribution for C budgets  
819 at catchment scale. We demonstrate that CE-DYNAM captures the spatial variability in soil erosion, C erosion and SOC  
820 stocks of the non-Alpine region of the Rhine catchment when compared to high-resolution estimates and observations. We  
821 also show that the quantile ranges of erosion and deposition rates and C stocks fall within the uncertainty ranges of  
822 previous estimates at basin or sub-basin level. Furthermore, we demonstrate the model ability to disentangle vertical C  
823 fluxes resulting from the redistribution of C over land and develop C budgets that can shed light on the role of erosion in  
824 the C cycle. The simple structure of CE-DYNAM and the relative low amount of parameters makes it possible to run  
825 several simulations to investigate the role of individual processes on the C cycle such as removal by erosion only, or the  
826 role of deposition and transport. Its compatibility with land surface models makes it possible to investigate the long-term  
827 and large-scale effect of erosion processes under various global changes such as increasing atmospheric CO<sub>2</sub>  
828 concentrations, changes to precipitation and temperature, and land use change.

829

830 The application of CE-DYNAM for the Rhine catchment for the period 1850-2005 AD reveals three key findings:

- 831 ● Soil erosion leads to a cumulative net C sink of 216±23 Tg by the end of the period, which is in the same order of  
832 magnitude as the cumulative land C sink of the Rhine without erosion. This C sink is a result of an increasing  
833 dynamic replacement of C on eroding sites due to the CO<sub>2</sub> fertilization effect, despite decreasing soil and C  
834 erosion rates over the largest part of the catchment. We conclude that it is important to take global changes such as  
835 climate change into account to better quantify the net effect of erosion on the C cycle.
- 836 ● After performing a sensitivity analysis on key model parameters we find that the C enrichment by erosion, crop  
837 residue management and a different spatial variability of the residence time of floodplain sediment can



838 substantially change the overall values of C fluxes and SOC storages. However, the main findings, such as soil  
839 erosion being a net C sink for the Rhine catchment, remain.

- 840 • Initial climate and land cover conditions and the transient period over which erosion under global changes takes  
841 place are essential for the determination if soil erosion is a net C sink or source and to what extent.

842  
843 Altogether, these results indicate that despite model uncertainties related to the relative coarse spatial resolution, missing or  
844 simplified processes, CE-DYNAM represents an important step forwards into integrating soil erosion processes and  
845 sediment dynamics in Earth system models. The next step would be to improve CE-DYNAM with respect to riverine  
846 sediment and POC export fluxes and management practices.

#### 847 848 **Code and data availability**

849  
850 The source code of CE-DYNAM is included as a supplement to this paper. Model data can be accessed from the Zenodo  
851 repository under the doi:10.5281/zenodo.2642452 (not published yet). For the other data sets that are listed in Table 1, it is  
852 encouraged to contact the first authors of the original references.

#### 853 854 **Author contributions**

855  
856 VN built and implemented the mode. YW provided the basic structure for the model. All authors contributed in the  
857 interpretation of the results and wrote the paper.

#### 858 859 **Competing interests**

860  
861 *The authors declare that they have no conflict of interest.*

#### 862 863 **Acknowledgements**

864  
865 Funding was provided by the Laboratory for Sciences of Climate and Environment (LSCE), CEA, CNRS, and UVSQ.  
866 Victoria Naipal, Ronny Lauerwald and Philippe Ciais acknowledges support from the VERIFY project that received  
867 funding from the European Union's Horizon 2020 research and innovation program under grant agreement No 776810.  
868 Bertrand Guenet acknowledges support from the project ERANETMED2-72-209 ASSESS. We also thank Dr. S. Peng for  
869 sharing the PFT maps.

#### 870 871 **References**

872  
873 Asselman, N. E. M.: Suspended sediment dynamics in a large drainage basin : the River Rhine , 1450(November 1998),

874 1437–1450, [https://doi.org/10.1002/\(SICI\)1099-1085\(199907\)13:10<1437::AID-HYP821>3.0.CO;2-J](https://doi.org/10.1002/(SICI)1099-1085(199907)13:10<1437::AID-HYP821>3.0.CO;2-J), 1999.

875

876 Asselman, N. E. M., Middelkoop, H. and van Dijk, P. M.: The impact of changes in climate and land use on soil erosion,  
877 transport and deposition of suspended sediment in the River Rhine, *Hydrol. Process.*, 17(16), 3225–3244,  
878 doi:10.1002/hyp.1384, 2003.

879

880 Ballabio, C., Panagos, P. and Monatanarella, L.: Geoderma Mapping topsoil physical properties at European scale using the  
881 LUCAS database, *Geoderma*, 261, 110–123, doi:10.1016/j.geoderma.2015.07.006, 2016.

882

883 Berhe, A. A., Harte, J., Harden, J. W. and Torn, M. S.: The Significance of the Erosion-induced Terrestrial Carbon Sink,  
884 *Bioscience*, 57(4), 337, doi:10.1641/B570408, 2007.

885

886 Berhe, A. A., Harden, J. W., Torn, M. S. and Harte, J.: Linking soil organic matter dynamics and erosion-induced terrestrial  
887 carbon sequestration at different landform positions, *J. Geophys. Res. Biogeosciences*, 113(4), 1–12,  
888 doi:10.1029/2008JG000751, 2008.

889

890 Beusen, A. H. W., Dekkers, A. L. M., Bouwman, A. F., Ludwig, W., & Harrison, J.: Estimation of global river transport of  
891 sediments and associated particulate C, N, and P, *Global Biogeochemical Cycles*, 19(4), doi:10.1029/2005GB002453,  
892 2005.

893

894 Billings, S. A., Richter, D. D. B., Ziegler, S. E., Prestegard, K. and Wade, A. M.: Distinct Contributions of Eroding and  
895 Depositional Profiles to Land-Atmosphere CO<sub>2</sub> Exchange in Two Contrasting Forests, 7(March),  
896 doi:10.3389/feart.2019.00036, 2019.

897

898 Borrelli, P., Van Oost, K., Meusburger, K., Alewell, C., Lugato, E., Panagos, P.: A step towards a holistic assessment of  
899 soil degradation in Europe: Coupling on-site erosion with sediment transfer and carbon fluxes, *Environmental Research*,  
900 161, 291-298, doi:<https://doi.org/10.1016/j.envres.2017.11.009>, 2018

901

902 de Brogniez, D., Ballabio, C., Stevens, A., Jones, R. J. A., Montanarella, L. and Van Wesemael, B.: A map of the topsoil  
903 organic carbon content of Europe generated by a generalized additive model, *Eur. J. Soil Sci.*, 66(January), 121–134,  
904 doi:10.1111/ejss.12193, 2015.

905

906 Bug, J., Stolz, W., Stegger, U.: Potentielle Erosionsgefaehrdung der Ackerboeden durch Wasser in Deutschland,  
907 Bundesanstalt fuer Geowissenschaften und Rohstoffe, [www.bgr.bund.de/Boden](http://www.bgr.bund.de/Boden), 2014

908

909 Cerdan, O., Govers, G., Le Bissonnais, Y., Van Oost, K., Poesen, J., Saby, N., Gobin, a., Vacca, a., Quinton, J.,

910 Auerswald, K., Klik, a., Kwaad, F. J. P. M., Raclot, D., Ionita, I., Rejman, J., Rouseva, S., Muxart, T., Roxo, M. J. and  
911 Dostal, T.: Rates and spatial variations of soil erosion in Europe: A study based on erosion plot data, *Geomorphology*,  
912 122(1–2), 167–177, doi:10.1016/j.geomorph.2010.06.011, 2010.

913

914 Ciais, P., Sabine, C., Bala, G., Bopp, L., Brovkin, V., Canadell, J., Chhabra, A., DeFries, R., Galloway, J., Heimann, M.,  
915 Jones, C., Quéré, C. Le, Myneni, R. B., Piao, S. and Thornton, P.: Carbon and Other Biogeochemical Cycles, in *Climate*  
916 *Change 2013: The physical science basis. Contribution of working group I to the fifth assessment report of the*  
917 *intergovernmental panel on climate change* [Stocker, T.F., D. Qin, G.-K. Plattner, M. Tignor, S.K. Allen, J. Boschung, A.  
918 Nauels, Y. Xia, pp. 465–570, Cambridge University Press, Cambridge, United Kingdom and New York, NY., 2013.

919

920 De Moor, J. J. W., & Verstraeten, G.: Alluvial and colluvial sediment storage in the Geul River catchment (The  
921 Netherlands)—combining field and modelling data to construct a Late Holocene sediment budget, *Geomorphology*,  
922 95(3-4), 487-503, 2008

923

924 Doetterl, S., Van Oost, K. and Six, J.: Towards constraining the magnitude of global agricultural sediment and soil organic  
925 carbon fluxes, *Earth Surf. Process. Landforms*, doi:10.1002/esp.3198, 2012.

926

927 Doetterl, S., Berhe, A. A., Nadeu, E., Wang, Z., Sommer, M., & Fiener, P.: Erosion, deposition and soil carbon: a review of  
928 process-level controls, experimental tools and models to address C cycling in dynamic landscapes, *Earth-Science Reviews*,  
929 154, 102-122, 2016.

930

931 Dotterweich, M.: *Geomorphology The history of human-induced soil erosion : Geomorphic legacies , early descriptions*  
932 *and research , and the development of soil conservation — A global synopsis*, *Geomorphology*, 201(November), 1–34,  
933 doi:10.1016/j.geomorph.2013.07.021, 2013.

934

935 Elliot, W. J.: WEPP INTERNET INTERFACES FOR FOREST EROSION PREDICTION 1, *JAWRA Journal of the*  
936 *American Water Resources Association*, 40(2), 299-309, 2004.

937

938 Erkens, G.: *Sediment dynamics in the Rhine catchment*, Utrecht University, Faculty of Geosciences, Utrecht., 2009.

939

940 Foster, G. R., Yoder, D. C., Weesies, G. A., McCool, D. K., McGregor, K. C., & Bingner, R. L.: *User’s Guide—revised*  
941 *universal soil loss equation version 2 (RUSLE 2)*. USDA–Agricultural Research Service, Washington, DC., 2002.

942

943 Frieler, K., Lange, S., Piontek, F., Reyser, C. P. O., Schewe, J., Warszawski, L., Zhao, F., Chini, L., Denvil, S., Emanuel, K.,  
944 Geiger, T., Halladay, K., Hurtt, G., Mengel, M., Murakami, D., Ostberg, S., Popp, A. and Riva, R.: *Assessing the impacts*  
945 *of 1.5 °C global warming – simulation protocol of the Inter-Sectoral Impact Model Intercomparison Project ( ISIMIP2b )*,

946 Geosci. Model Dev., 10, 4321–4345, 2017.

947

948 Galy, V., Peucker-Ehrenbrink, B., & Eglinton, T. Global carbon export from the terrestrial biosphere controlled by erosion.

949 Nature, 521, 204–207. <https://doi.org/10.1038/nature14400>, 2015.

950

951 Guenet, B., Camino-Serrano, M., Ciais, P., Tifafi, M., Maignan, F., Soong, J. L., & Janssens, I. A.: Impact of

952 priming on global soil carbon stocks, *Global change biology*, 24(5), 1873–1883, 2018.

953

954 Gumiere, S. J., Le Bissonnais, Y., Raclot, D., & Cheviron, B.: Vegetated filter effects on sedimentological connectivity of

955 agricultural catchments in erosion modelling: a review. *Earth Surface Processes and Landforms*, 36(1), 3–19, 2011.

956

957 Hay R.K.M.: Harvest index: a review of its use in plant breeding and crop physiology, *Ann. appl. Biol.*, 126, 197–216,

958 1995.

959

960 Hoffmann, T., Erkens, G., Cohen, K. M., Houben, P., Seidel, J. and Dikau, R.: Holocene floodplain sediment storage and

961 hillslope erosion within the Rhine catchment, *The Holocene*, 17(1), 105–118, doi:10.1177/0959683607073287, 2007.

962

963 Hoffmann, T., Lang, a and Dikau, R.: Holocene river activity: analysing 14C-dated fluvial and colluvial sediments from

964 Germany, *Quat. Sci. Rev.*, 27(21–22), 2031–2040, doi:10.1016/j.quascirev.2008.06.014, 2008.

965

966 Hoffmann, T., Schlummer, M., Notebaert, B., Verstraeten, G. and Korup, O.: Carbon burial in soil sediments from

967 Holocene agricultural erosion, Central Europe, *Global Biogeochem. Cycles*, 27(3), 828–835, doi:10.1002/gbc.20071,

968 2013a.

969

970 Hoffmann, T., Mudd, S. M., van Oost, K., Verstraeten, G., Erkens, G., Lang, a., Middelkoop, H., Boyle, J., Kaplan, J. O.,

971 Willenbring, J. and Aalto, R.: Short Communication: Humans and the missing C-sink: erosion and burial of soil carbon

972 through time, *Earth Surf. Dyn.*, 1(1), 45–52, doi:10.5194/esurf-1-45-2013, 2013b.

973

974 Hurtt, G. C., Chini, L. P., Frohking, S., Betts, R. A., Feddema, J. and Fischer, G.: Harmonization of land-use scenarios for

975 the period 1500 – 2100 : 600 years of global gridded annual land-use transitions , wood harvest , and resulting secondary

976 lands, *Clim. Chang.*, 109, 117–161, doi:10.1007/s10584-011-0153-2, 2011.

977

978 Kinnell, P. I. A.: Runoff dependent erosivity and slope length factors suitable for modelling annual erosion using the

979 Universal Soil Loss Equation. *Hydrological Processes: An International Journal*, 21(20), 2681–2689, 2007.

980

981 Krinner, G., Viovy, N., de Noblet-Ducoudré, N., Ogée, J., Polcher, J., Friedlingstein, P., Ciais, P., Sitch, S. and Prentice, I.

982 C.: A dynamic global vegetation model for studies of the coupled atmosphere-biosphere system, *Global Biogeochem.*  
983 *Cycles*, 19(1), 1–33, doi:10.1029/2003GB002199, 2005.

984

985 Lal, R.: Soil erosion and the global carbon budget., *Environ. Int.*, 29(4), 437–50, doi:10.1016/S0160-4120(02)00192-7,  
986 2003.

987

988 Lehner, B. and Grill, G.: Global river hydrography and network routing : baseline data and new approaches to study the  
989 world ' s large river systems, *Hydrol. Process.*, 2186(April), 2171–2186, doi:10.1002/hyp.9740, 2013.

990

991 Ludwig, W. and Probst, J.-L.: River Sediment Discharge to the Oceans: Present-Day Controls and Global Budgets, *Am. J.*  
992 *Sci.*, 298(April), 265–295, 1998.

993

994 Lugato, E., Smith, P., Borrelli, P., Panagos, P., Ballabio, C., Orgiazzi, A., Fernandez-ugalde, O., Montanarella, L. and  
995 Jones, A.: Soil erosion is unlikely to drive a future carbon sink in Europe, *Sci. Adv.*, 4(November), eaau3523, 2018.

996

997 Martínez-mena, M., Almagro, M., García-franco, N., Vente, J. De and García, E.: Fluvial sedimentary deposits as carbon  
998 sinks : organic carbon pools and stabilization mechanisms across a Mediterranean catchment, 1035–1051, 2019.

999

1000 Mayorga, E., Seitzinger, S. P., Harrison, J. a., Dumont, E., Beusen, A. H. W., Bouwman, a. F., Fekete, B. M., Kroeze, C.  
1001 and Van Drecht, G.: Global Nutrient Export from WaterSheds 2 (NEWS 2): Model development and implementation,  
1002 *Environ. Model. Softw.*, 25(7), 837–853, doi:10.1016/j.envsoft.2010.01.007, 2010.

1003

1004 Müller, C., Elliott, J., Kelly, D., Arneith, A., Balkovic, J., Ciais, P., ... & Jones, C. D.: The Global Gridded Crop Model  
1005 Intercomparison phase 1 simulation dataset, *Scientific data*, 6(1), 50, 2019.

1006

1007 Nadeu, E., Gobin, A., Fiener, P., van Wesemael, B. and van Oost, K.: Modelling the impact of agricultural management on  
1008 soil carbon stocks at the regional scale: the role of lateral fluxes., *Glob. Chang. Biol.*, 21(8), 3181–92,  
1009 doi:10.1111/gcb.12889, 2015.

1010

1011 Naipal, V., Reick, C., Pongratz, J. and Van Oost, K.: Improving the global applicability of the RUSLE model - Adjustment  
1012 of the topographical and rainfall erosivity factors, *Geosci. Model Dev.*, 8(9), doi:10.5194/gmd-8-2893-2015, 2015.

1013

1014 Naipal, V., Reick, C., Van Oost, K., Hoffmann, T. and Pongratz, J.: Modeling long-term, large-scale sediment storage using  
1015 a simple sediment budget approach, *Earth Surf. Dyn.*, 4, 407–423, doi:10.5194/esurf-4-407-2016, 2016.

1016

1017 Naipal, V., Ciais, P., Wang, Y., Lauerwald, R., Guenet, B. and Oost, K. Van: Global soil organic carbon removal by water

1018 erosion under climate change and land use change during AD 1850 – 2005, *Biogeosciences*, 15(July), 4459–4480,  
1019 doi:<https://doi.org/10.5194/bg-15-4459-2018>, 2018.

1020

1021 Van Oost, K., Quine, T. a, Govers, G., De Gryze, S., Six, J., Harden, J. W., Ritchie, J. C., McCarty, G. W., Heckrath, G.,  
1022 Kosmas, C., Giraldez, J. V, da Silva, J. R. M. and Merckx, R.: The impact of agricultural soil erosion on the global carbon  
1023 cycle., *Science*, 318(5850), 626–9, doi:10.1126/science.1145724, 2007.

1024

1025 Van Oost, K., Verstraeten, G., Doetterl, S., Notebaert, B., Wiaux, F. and Broothaerts, N.: Legacy of human-induced C  
1026 erosion and burial on soil – atmosphere C exchange, *PNAS*, 109(47), 19492–19497,  
1027 doi:10.1073/pnas.1211162109/-/DCSupplemental.[www.pnas.org/cgi/doi/10.1073/pnas.1211162109](http://www.pnas.org/cgi/doi/10.1073/pnas.1211162109), 2012.

1028

1029 Palmieri, A., Martino, L., Dominici, P. and Kasanko, M.: Land Cover and Land Use Diversity Indicators in LUCAS 2009  
1030 data., 2011.

1031

1032 Panagos, P., Borrelli, P., Poesen, J., Ballabio, C., Lugato, E., Meusburger, K., Montanarella, L. and Alewell, C.:  
1033 Environmental Science & Policy The new assessment of soil loss by water erosion in Europe, *Environ. Sci. Policy*, 54,  
1034 438–447, doi:10.1016/j.envsci.2015.08.012, 2015.

1035

1036 Panagos, P., Borrelli, P., Meusburger, K., Yu, B., Klik, A., Lim, K. J., Yang, J. E., Ni, J., Miao, C., Chattopadhyay, N.,  
1037 Sadeghi, S. H., Hazbavi, Z., Zabihi, M., Larionov, G. A., Krasnov, S. F., Gorobets, A. V., Levi, Y., Erpul, G., Birkel, C.,  
1038 Hoyos, N., Naipal, V., Oliveira, P. T. S., Bonilla, C. A., Meddi, M., Nel, W., Al Dashti, H., Boni, M., Diodato, N., Van  
1039 Oost, K., Nearing, M. and Ballabio, C.: Global rainfall erosivity assessment based on high-temporal resolution rainfall  
1040 records, *Sci. Rep.*, 7(1), doi:10.1038/s41598-017-04282-8, 2017.

1041

1042 Parton, W. J., Schimel, D. S., Cole, C. V. and Ojima, D. S.: Analysis of Factors Controlling Soil Organic Matter Levels in  
1043 Great Plains Grasslands1, *Soil Sci. Soc. Am. J.*, 51(5), 1173, doi:10.2136/sssaj1987.03615995005100050015x, 1987.

1044

1045 Pelletier, J. D.: A spatially distributed model for the long-term suspended sediment discharge and delivery ratio of drainage  
1046 basins, *J. Geophys. Res., Earth Surface* 117 (F2), doi: <https://doi.org/10.1029/2011JF002129>, 2012.

1047

1048 Pelletier, J. D., Broxton, P. D., Hazenberg, P., Zeng, X., Troch, P. A., Niu, G. Y., Williams, Z., Brunke, M. A. and Gochis,  
1049 D.: A gridded global data set of soil, intact regolith, and sedimentary deposit thicknesses for regional and global land  
1050 surface modeling, *J. Adv. Model. Earth Syst.*, doi:10.1002/2015MS000526, 2016.

1051

1052 Peng, S., Ciais, P., Maignan, F., Li, W., Chang, J., Wang, T. and Yue, C.: Sensitivity of land use change emission estimates

1053 to historical land use and land cover mapping, *Global Biogeochem. Cycles*, 31(4), 626–643, doi:10.1002/2015GB005360,  
1054 2017.

1055

1056 Renard, K. G., & Ferreira, V. A.: RUSLE model description and database sensitivity. *Journal of environmental quality*,  
1057 22(3), 458-466, 1993.

1058

1059 Renard, K.G., Foster, G.R., Weesies, G.A., McCool, D.K., Yoder, D. C.: *Predicting Soil Erosion by Water: A Guide to*  
1060 *Conservation Planning with the Revised Universal Soil Loss Equation (RUSLE)*, United States Department of Agriculture,  
1061 Washington, DC., 1997.

1062

1063 Schauburger, B., Ben-ari, T., Makowski, D., Kato, T., Kato, H. and Ciais, P.: Yield trends , variability and stagnation  
1064 analysis of major crops in France over more than a century, *Sci. Rep.*, (November), 1–12,  
1065 doi:10.1038/s41598-018-35351-1, 2018.

1066

1067 Shangguan H.W., Dai Y., Duan Q., Liu B., Y. H.: A global soil data set for earth system modeling Wei, J. *Adv. Model.*  
1068 *Earth Syst.*, 6, 249–263, 2014, doi:10.1002/2013MS000293.

1069

1070 Sorribas, M. V., da Motta Marques, D., Castro, N. M. D. R., & Fan, F. M.: Fluvial carbon export and CO<sub>2</sub> efflux in  
1071 representative nested headwater catchments of the eastern La Plata River Basin, *Hydrological processes*, 31(5), 995-1006,  
1072 2017.

1073

1074 Stallard, R. F.: Terrestrial sedimentation and the carbon cycle : Coupling weathering and erosion to carbon burial, *Global*  
1075 *Biogeochem. Cycles*, 12(2), 231–257, 1998.

1076

1077 Tan, Z., Leung, L. R., Li, H., Tesfa, T., Vanmaercke, M., Poesen, J., ... Hartmann, J. A Global data analysis for representing  
1078 sediment and particulate organic C carbon yield in Earth System Models. *Water Resources Research*, 53, 10,674–10,700.  
1079 <https://doi.org/10.1002/2017WR020806>, 2017

1080

1081 Thonicke, K., Spessa, A., Prentice, I. C., Harrison, S. P. and Dong, L.: The influence of vegetation , fire spread and fire  
1082 behaviour on biomass burning and trace gas emissions: results from a process-based model, *Biogeosciences*, 7,  
1083 1991–2011, doi:10.5194/bg-7-1991-2010, 2010.

1084

1085 Todd-Brown, K. E., Randerson, J. T., Post, W. M., Hoffman, F. M., Tarnocai, C., Schuur, E. A., & Allison, S. D.: Causes of  
1086 variation in soil carbon simulations from CMIP5 Earth system models and comparison with observations, *Biogeosciences*  
1087 (10), 1717-1736, 10.5194/bg-10-1717-2013, 2013.

1088

1089 Wang, Z., Govers, G., Steegen, A., Clymans, W., Putte, A. Van Den, Langhans, C., Merckx, R. and Oost, K. Van:  
1090 Geomorphology Catchment-scale carbon redistribution and delivery by water erosion in an intensively cultivated area,  
1091 Geomorphology, 124(1–2), 65–74, doi:10.1016/j.geomorph.2010.08.010, 2010.  
1092

1093 Wang, Z., Doetterl, S., Vanclooster, M., van Wesemael, B. and Van Oost, K.: Constraining a coupled erosion and soil  
1094 organic carbon model using hillslope-scale patterns of carbon stocks and pool composition, J. Geophys. Res.  
1095 Biogeosciences, 120, 452–465, doi:10.1002/2014JG002768, 2015.  
1096

1097 Wang, Z., Hoffmann, T., Six, J., Kaplan, J. O., Govers, G., Doetterl, S. and Van Oost, K.: Human-induced erosion has  
1098 offset one-third of carbon emissions from land cover change, Nat. Clim. Chang., 7(5), 345–349, doi:10.1038/nclimate3263,  
1099 2017.  
1100

1101 Wiesmeier, M., Sporlein, P., Geuß, U. W. E., Hangen, E., Haug, S., Reischl, A., Schilling, B., Lutzow, M. V. O. N. and  
1102 Kogel-Knaber, I.: Soil organic carbon stocks in southeast Germany ( Bavaria ) as affected by land use , soil type and  
1103 sampling depth, Glob. Chang. Biol., (March), 1–13, doi:10.1111/j.1365-2486.2012.02699.x, 2012.  
1104  
1105  
1106  
1107  
1108  
1109  
1110  
1111  
1112  
1113  
1114  
1115  
1116  
1117  
1118  
1119  
1120  
1121  
1122  
1123  
1124



1125 **Table 1:** Model input datasets

Dataset	Spatial resolution	Temporal resolution	Period	Source
Historical land cover and land use change	0.25 degrees	annual	1850-2005	Peng et al. (2017)
Climate data (precipitation & temperature) for ORCHIDEE	0.5 degrees	6 hourly	1900-2012	CRU-NCEP version 5.3.2; <a href="https://crudata.uea.ac.uk/cru/data/ncep/">https://crudata.uea.ac.uk/cru/data/ncep/</a> ; last access: 5 April 2019
precipitation for the Adj. RUSLE	0.5 degrees	monthly	1850-2005	ISIMIP2b (Frieler et al., 2017)
Soil	1 km	-	-	Global Soil Dataset for Earth System Modeling, GSDE (Shangguan H.W., Dai Y., Duan Q., Liu B., 2014)
Topography	30 arcseconds	-	-	GTOPO30; U.S. Geological Survey, EROS Data Center Distributed Active Archive Center 2004; <a href="https://www.ngdc.noaa.gov/mgg/topo/gltiles.html">https://www.ngdc.noaa.gov/mgg/topo/gltiles.html</a> ; last access: 5 April 2019
Flow accumulation	30 arcseconds	-	-	HydroSHEDS (Lehner et al., 2013); <a href="https://www.hydrosheds.org/">https://www.hydrosheds.org/</a> ; last access: 5 April 2019
Hillslopes/Floodplain area	5 arcminutes	-	-	Pelletier et al. (2016)
River network & stream length	30 arcseconds	-	-	Hydrosheds (Lehner et al., 2008)

1126  
 1127 **Table 2:** Model simulations, with changes to the basin average gross soil erosion rate ( $t\ ha^{-1}\ y^{-1}$ ), the basin average  
 1128 sediment residence time Tau (years), and the enrichment factor, and the crop residue harvest intensity, RM (%).

Default simulations	Gross soil erosion	Tau	Enrichment factor	RM
S0	0	-	-	0
S1	3.94	94	1	0
S2	3.94	94	1	0
<b>Uncertainty simulations</b>				
S1_min	1.52	94	1	0
S2_min	1.52	94	1	0
S1_max	5.95	94	1	0
S2_max	5.95	94	1	0
<b>Sensitivity</b>				

<b>simulations</b>				
S2_Tmin	3.94	60	1	0
S2_Tmax	4.94	128	1	0
S1_EF	5.94	94	2	0
S2_EF	6.94	94	2	0
S0_RM	0	-	-	100
S1_RM	3.94	94	1	100
S2_RM	3.94	94	1	100

1129  
1130 **Table 3:** Goodness-of-fit results of the comparison of the simulated gross and net erosion rates to those of other studies at  
1131 subbasin level, taking into account 13 sub-basins of the Rhine. RMSE is the root mean square error in  $10^6$  tons year<sup>-1</sup>. E  
1132 stands for soil erosion.

	E Cerdan et al. (2010)	E Germany	E RUSLE2015	E Borrelli et al. (2018)
<i>r-squared</i>	0.72	0.97	0.94	0.24
<i>RMSE</i>	0.68	1.98	0.92	1.35

1133  
1134 **Table 4:** Goodness-of-fit results of the comparison of the simulated gross and net C erosion rates to those of the study of  
1135 Lugato et al. (2018) in the enhanced and reduced scenario, taking into account 13 sub-basins of the Rhine. RMSE is the  
1136 root mean square error in tons year<sup>-1</sup>. Ce stands for gross C erosion, while Cd stands for net C erosion.

	Ce enhanced	Ce reduced	Cd enhanced	Cd reduced
<i>r-squared</i>	0.95	0.95	0.98	0.98
<i>RMSE</i>	7977	13797	3450	9822

1137  
1138 **Table 5:** This table shows the results of the linear regression between the simulated total SOC stocks (Tg of C per year)  
1139 and those of the Global Soil dataset for Earth System Modeling (GSDE) and from the LUCAS database. The regression is  
1140 done after aggregating the data at sub-basin level for the 13 sub-basins that were delineated in the Rhine catchment.  
1141 RMSE is the root mean square error given in Tg of C per year, while the r-value is the spatial correlation coefficient.

Regression	r-value	p-value	RMSE
This study versus LUCAS	0.96	<0.01	28.69
This study versus GSDE	0.95	<0.01	29.32

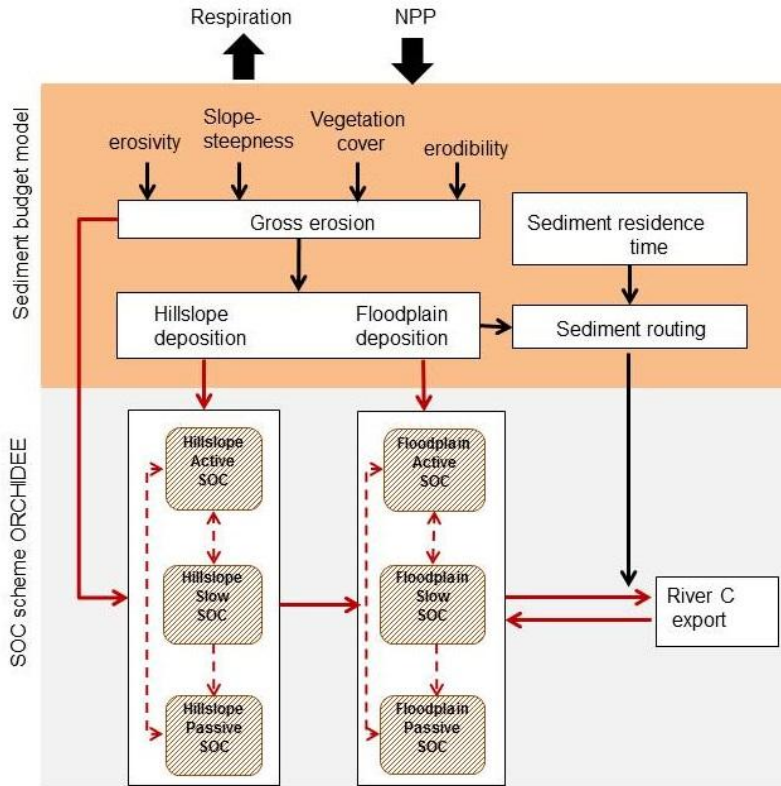
1143 **Table 6:** This table presents the scaling exponent (b) of equation 20 for floodplains and hillslopes. The scaling exponent  
 1144 was derived for selected points in the Rhine catchment for which measurements on the SOC storage were taken by  
 1145 Hoffmann et al. (2013), and at sub-basin level after the data on area and SOC stocks was aggregated for each of the 13  
 1146 sub-basins of the Rhine.

	Scaling exponent floodplains	Scaling exponent hillslopes
Hoffmann et al. (2013)	1.23±0.06	1.08±0.07
This study (selected points where measurements were taken)	1.14	0.83
This study (based on the 13 sub-basins)	1.06	1.00

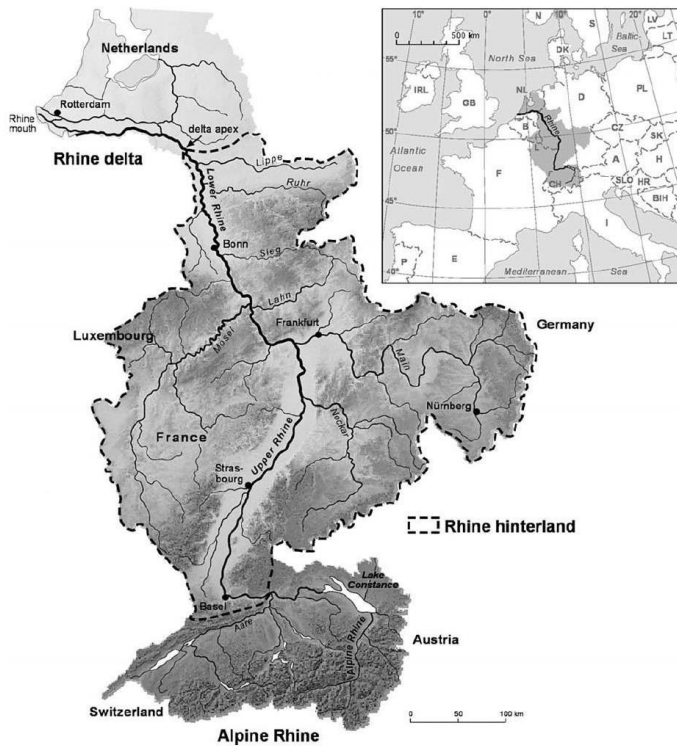
1147  
 1148 **Table 7:** Sensitivity analysis. The impacts of enrichment, changes to the sediment residence time ( $\tau_{min}$ ,  $\tau_{max}$ ), and crop  
 1149 residue management (RM) on the cumulative gross C erosion ( $C_e$ ), the cumulative change in the total SOC stock ( $dSOC$ ), the  
 1150 net C sink and the cumulative particulate organic C export flux ( $POC_{exp}$ ) of the Rhine catchment. Units: Tg C

	$C_e$	dSOC	C sink/source	$POC_{exp}$
<b>Default</b>	66	142	216	0.138
<b>enrichment</b>	106	198	271	0.137
<b><math>\tau_{min}</math></b>	66	130	204	0.198
<b><math>\tau_{max}</math></b>	66	100	173	0.117
<b>RM</b>	52	105	194	0.134

1151

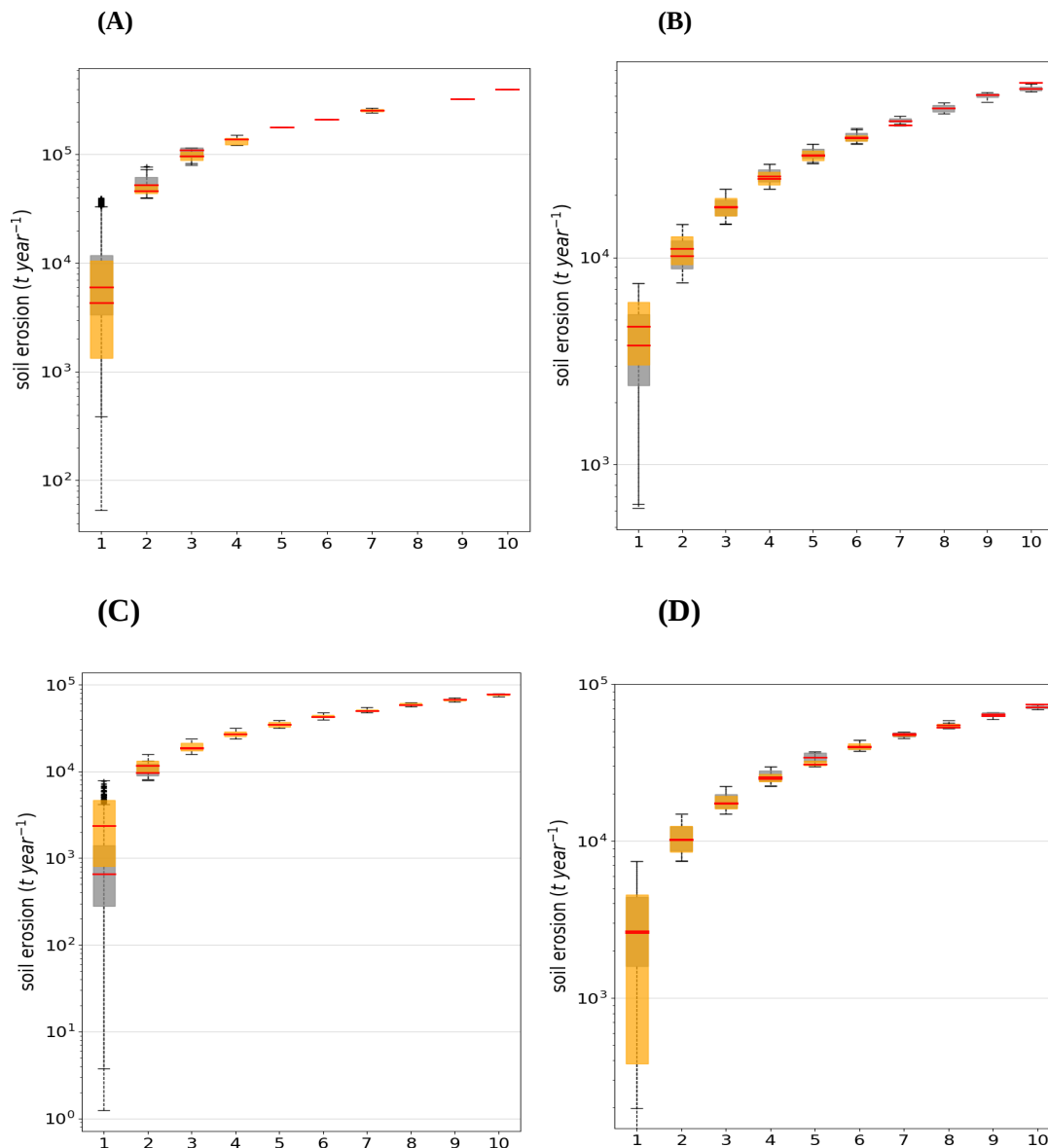


1153 **Figure 1:** A conceptual diagram of CE-DYNAM. The red arrows represent the C fluxes between the C pools/reservoirs,  
 1154 while the black arrows represent the link between the erosion processes (removal, deposition and transport).  
 1155



1156 **Figure 2:** The Rhine catchment (Hoffmann et al., 2013), where the gray shades represent elevation and the continuous  
1157 black lines the main rivers.

1158  
1159



1160

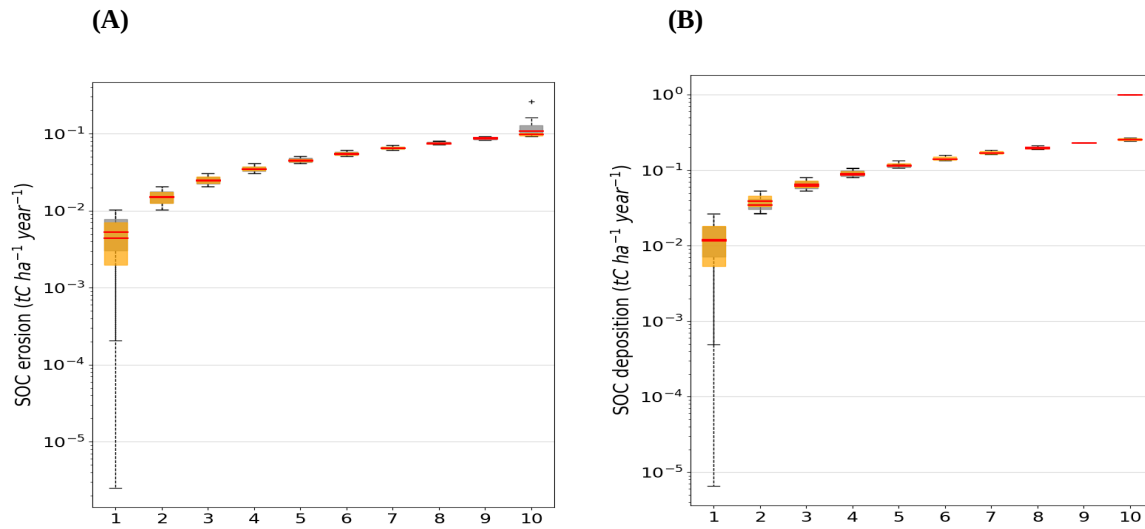
1161

1162 **Figure 3:** Quantile-whisker plot of simulated **gross** soil erosion rates (t/year) (grey whisker boxes), compared to (A) the  
1163 study of Cerdan et al. (2010), (B) the study of Panagos et al. (2015), and (C) the German potential erosion map by Bug et  
1164 al. (2014) (orange whisker boxes). (D) Quantile-whisker plot of simulated **net** soil erosion rates (t/year) (grey whisker  
1165 boxes), compared to the study of Borrelli et al. (2018) (orange whisker boxes). Medians are plotted as red horizontal lines.  
1166 The x-axis represents bins or evenly spaced ranges between the minimum and maximum total yearly soil erosion rates of  
1167 the Rhine.

1168

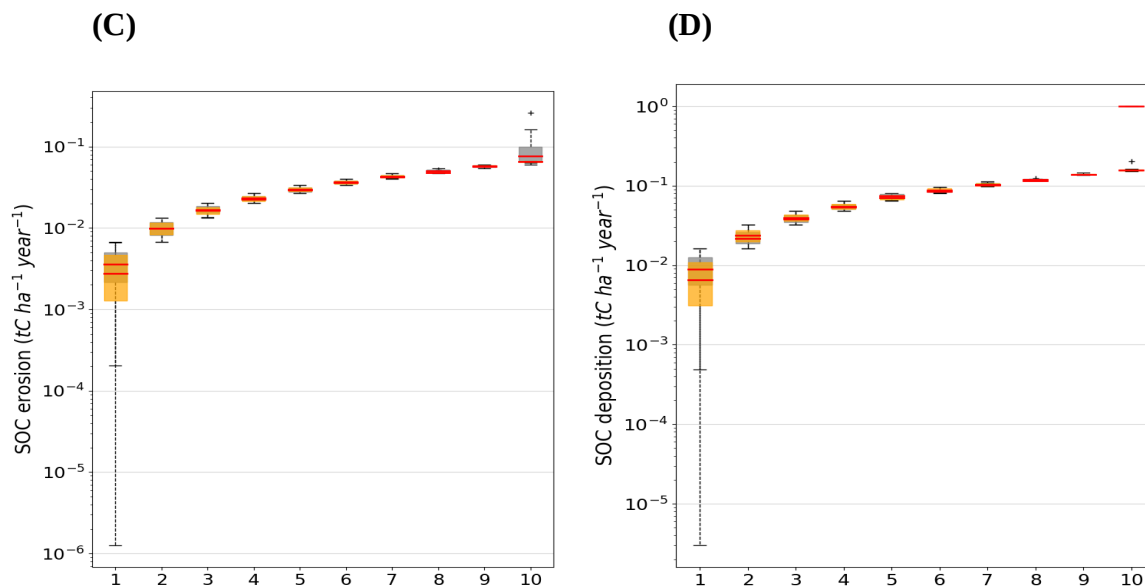
1169

1170



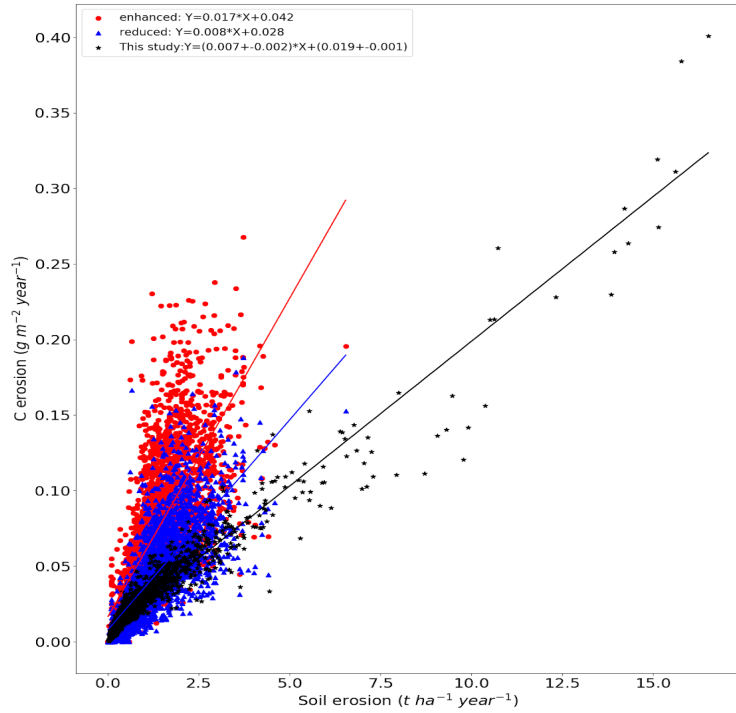
1171

1172



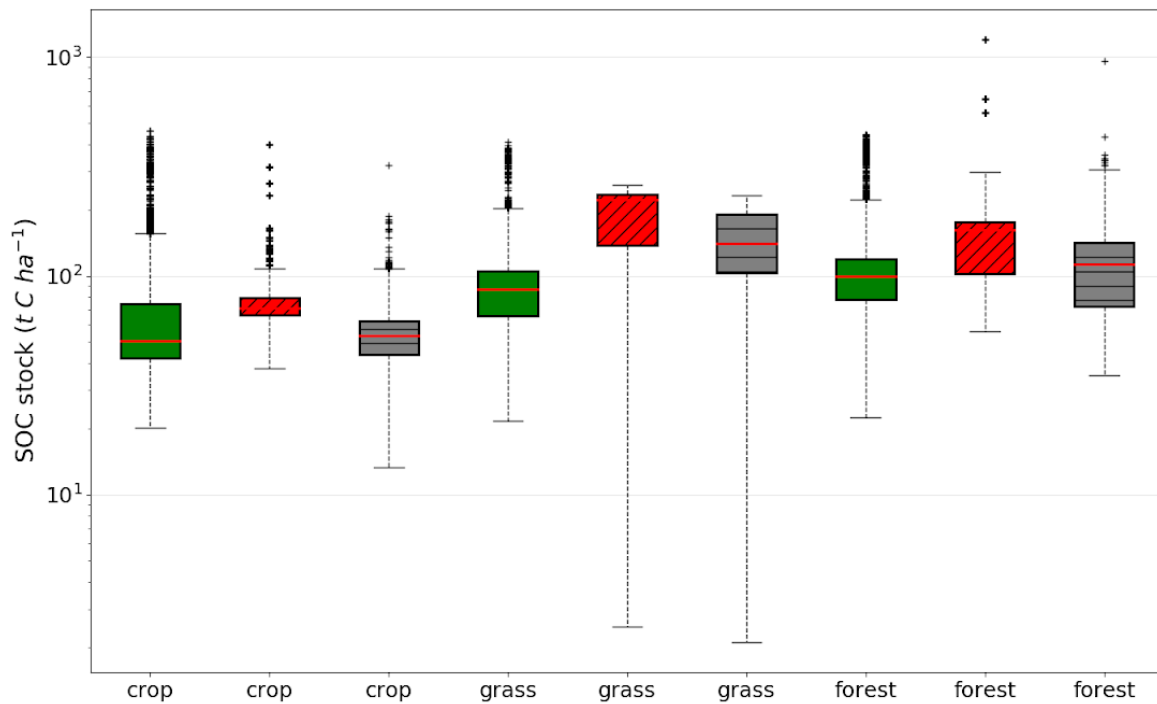
1173 **Figure 4:** (A) Hillslope C erosion rates and, (B) C deposition rates, compared to the enhanced erosion scenario from  
1174 Lugato et al. (2018). (C) Hillslope C erosion rates and, (D) C deposition rates, compared to the reduced erosion scenario  
1175 from Lugato et al. (2018). The x-axis represents bins or evenly spaced ranges between the minimum and maximum total  
1176 yearly soil erosion rates of the Rhine.

1177



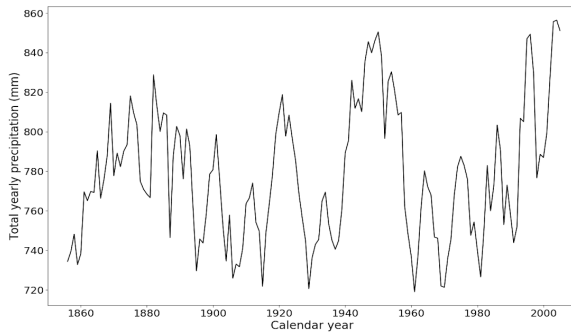
1178 **Figure 5:** The relationship between soil erosion and C erosion of simulation S2 (blackstars) in comparison to the erosion  
 1179 scenarios from the study of Lugato et al. (2018) with enhanced (red circles) and reduced erosion (blue triangles),  
 1180 respectively. The straight lines are the trendlines of the linear regression between soil and C erosion.

1181

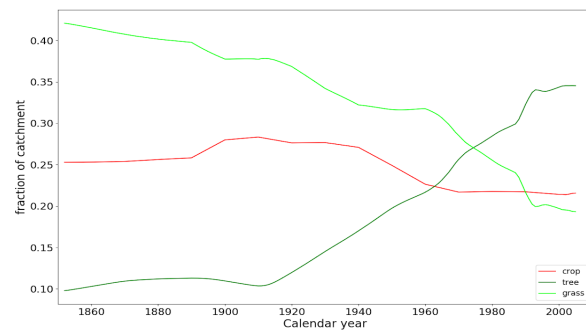


1182 **Figure 6:** Comparison of the total SOC stocks per land cover type between the simulation without erosion (red boxes with  
 1183 a ‘//’ pattern), the simulation with erosion (black boxes with a ‘-’ pattern) and the LUCAS data (green boxes without  
 1184 pattern fill). The red horizontal lines are the medians, the dashed vertical lines represent the range between the minimum  
 1185 and maximum, and the black dots are the outliers.

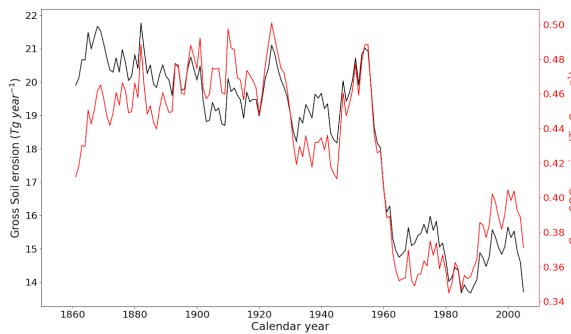
1186 (A)  
 1187



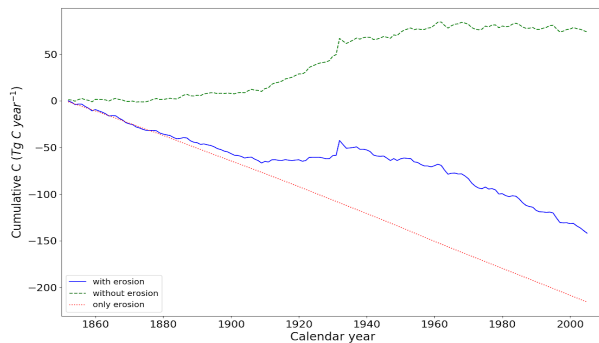
(B)



1188 (C)  
 1189

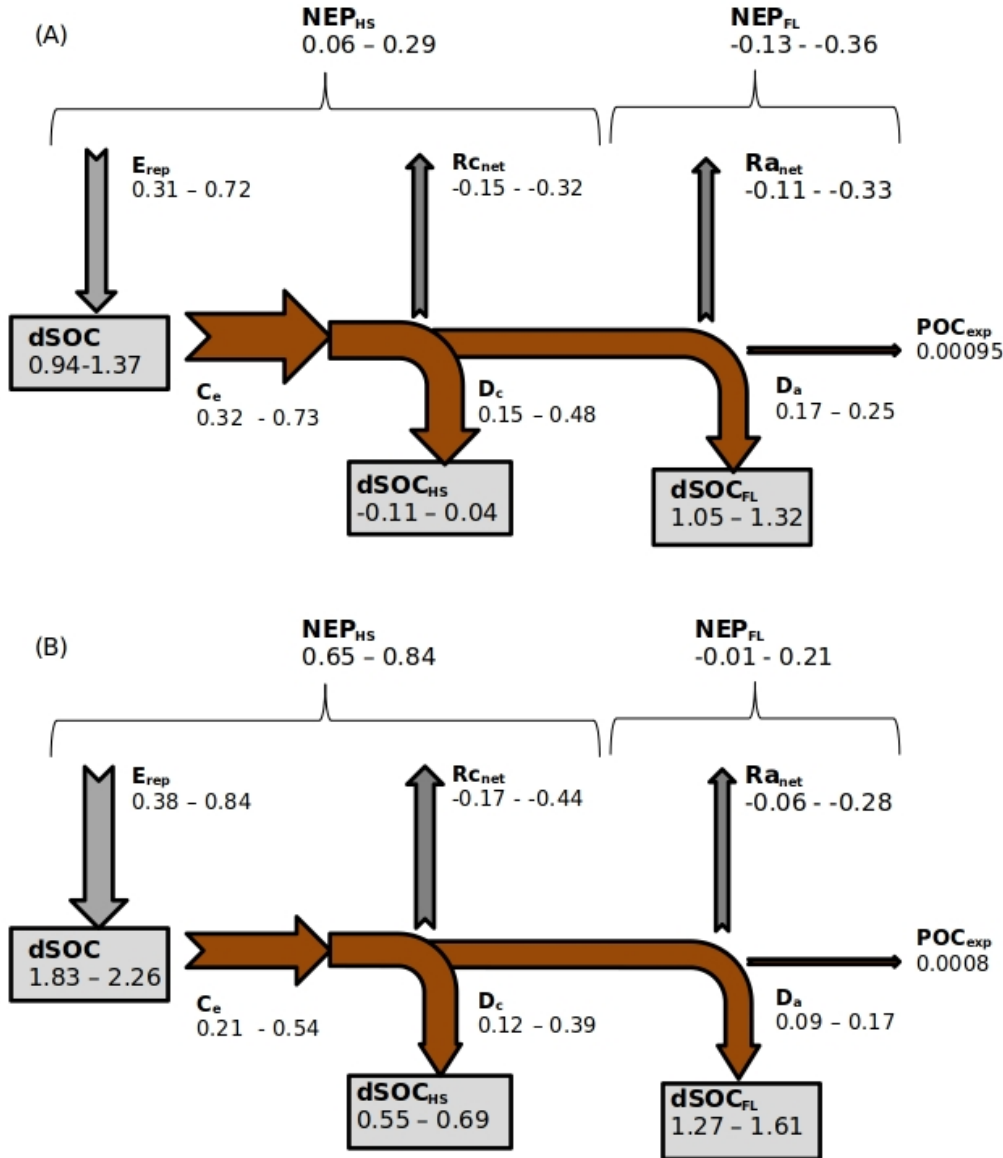


(D)



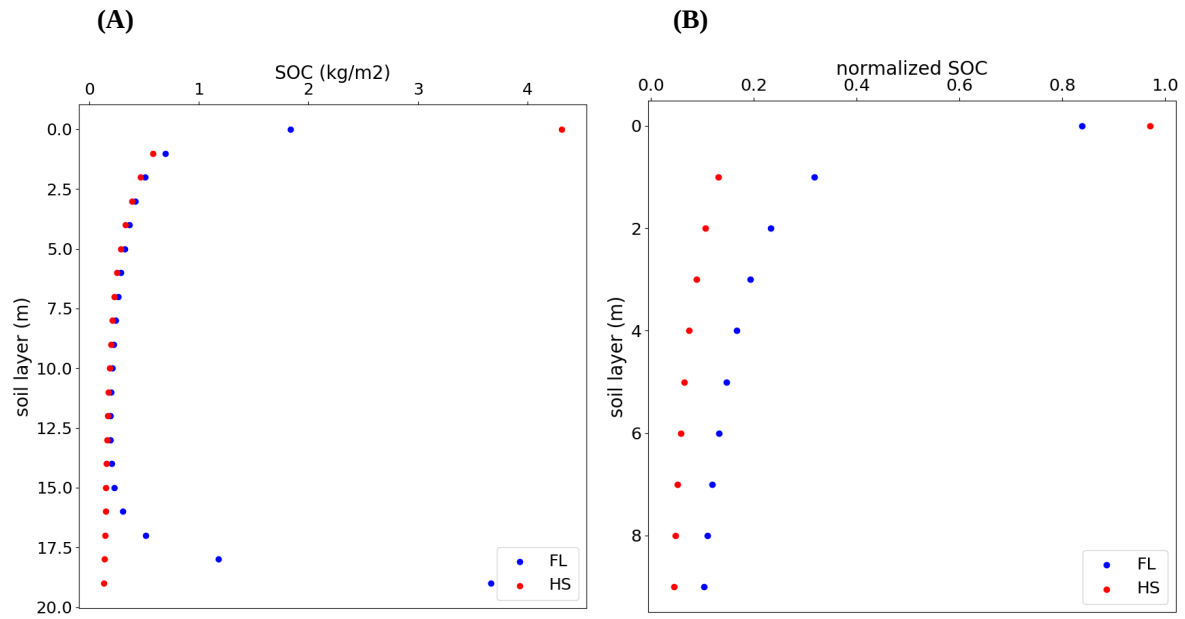
1190 **Figure 7:** Timeseries of (A) the 5-year average yearly precipitation (mm), (B) changing land cover fractions, (C): 5-year  
 1191 average total gross soil erosion ( $\text{Pg year}^{-1}$ ) and total gross C erosion rates ( $\text{Tg C year}^{-1}$ ), (D): Cumulative C emissions from  
 1192 the soil to the atmosphere under land use change and climate change without soil erosion (green dashed line), with soil  
 1193 erosion (blue straight line), due to additional respiration or stabilization of buried soil and photosynthetic replacement of C  
 1194 under erosion ( $E_p$ , red dotted line). All graphs represent the non-Alpine region of the Rhine catchment.





1196 **Figure 8:** (A) C budget of the non-Alpine part of the Rhine for the period 1851-1861, and (B) for the period 1995-2005.  
 1197 The budget shows the net exchange of C ( $Tg\ C\ year^{-1}$ ) between the soil and atmosphere as a result of accelerated soil  
 1198 erosion rates. Grey arrows are the erosion-induced yearly average **vertical** C fluxes, while the brown arrows are the  
 1199 erosion-induced yearly average **lateral** C fluxes.  $C_e$ : Gross C erosion from hillslopes;  $D_c$ : Deposition of C on hillslopes;  
 1200  $D_a$ : Deposition of C in floodplains;  $POC_{exp}$ : net POC export flux;  $E_p$ : Erosion-induced C replacement on hillslopes (Eq. 21);  
 1201  $R_{a_{net}}$ : Net respiration/burial of deposited C in floodplains (Eq. 23);  $R_{c_{net}}$ : Net respiration/burial of deposited C on hillslopes  
 1202 (Eq. 22);  $NEP_{HS}$ : Net ecosystem productivity of hillslopes;  $NEP_{FL}$ : Net ecosystem productivity of floodplains; The grey  
 1203 boxes represent yearly average changes in SOC stocks for the specific time period as a result of land use change, climate  
 1204 change, erosion and deposition.  $dSOC$ : Yearly average change in the total SOC stock;  $dSOC_{HS}$ : Yearly average change in  
 1205 the hillslope SOC stock;  $dSOC_{FL}$ : Yearly average change in the floodplain SOC stock.

1206  
1207



1208 **Figure 9:** (A) Vertical distribution of hillslope (red) and floodplain (blue) SOC stocks ( $\text{kg m}^{-2}$ ) with depth averaged over  
1209 the non-Alpine region of the Rhine catchment, and (B) the vertical distribution of normalized hillslope (red) and floodplain  
1210 (blue) SOC stocks (dimensionless) with depth.